ABSTRACT

Title of Thesis: USING A BURNING RATE EMULATOR TO ANALYZE FLAME EXTINCTION TIME ON THE INTERNATIONAL SPACE STATION

Anna Elizabeth Wright
Master of Science, 2021

Thesis Directed By: Dr. Peter Sunderland, Professor
Department of Fire Protection Engineering

There is limited understanding of the fire hazards in microgravity. As one of NASA's Advanced Combustion in Microgravity Experiments, the Burning Rate Emulator (BRE) is used to improve the understanding of material flammability in microgravity, including conditions that affect extinction behavior. Oscillation onset and extinction times were measured for emulated flames burning gaseous ethylene and methane diluted with nitrogen using two BRE burners aboard the International Space Station. Tests were performed with varying fuel flow rates, oxygen mole fractions (X_{O2}) between 0.21-0.4, and pressures between 0.57-1 bar. Relationships between extinction times and experimental parameters were explored to determine what conditions produce longer lasting flames. The measurements are correlated by scaling the times with $X_{O2}^3\,\mathrm{Re}^{-0.5}$, where Re is the jet Reynolds number. These times decrease with increasing burner diameter but are independent of pressure. This is further support of the significant hazards of using enriched oxygen atmospheres in spacecraft.

USING A BURNING RATE EMULATOR TO ANALYZE FLAME EXTINCTION TIMES ON THE INTERNATIONAL SPACE STATION

by

Anna Elizabeth Wright

Thesis submitted to the Faculty of the Graduate School of the
University of Maryland, College Park, in partial fulfillment
of the requirements for the degree of
Master of Science
2021

Advisory Committee:
Peter Sunderland, Professor, Chair
Stanislav Stoliarov, Professor
Arnaud Trouve, Professor

Acknowledgements

I am very grateful of all the support I received throughout my time on this project. I would like to extend my gratitude to Dr. Peter Sunderland for bringing me on the BRE team and for his guidance during the past year and a half. His ideas resulted in the completion of this work, and his passion for research is truly inspiring. I am confident that I am a better researcher because of him.

I would also like to thank members of the BRE team, past and present, for providing me with the tools needed to complete this work. I am especially grateful for Parham Dehghani for his constant assistance whenever I needed help. Thank you to Dr. John de Ris for sharing his thoughts and ideas with me on a weekly basis. Thank you to Dr. James Quintiere for sharing his knowledge with me and for all of his support. Thank you to Liora Mervis for her help with extinction time data collection, and for Aviv Kalai for their help with image sequence editing. This investigation was funded by NASA's ISS Research Program through agreement 80NSSC20M0119. I would also like to recognize Drs. Stanislav Stoliarov and Arnaud Trouve for agreeing to be members on my committee.

Thank you to my fellow FPE classmates who quickly became friends and the best support system I could ask for. I would especially like to thank Dani Knox, Libby Norwood, Kate Donlin, Joe Decker, and Jenn Wood for becoming a major part of my graduate school experience and making even the hard days enjoyable.

Finally, I am extremely thankful for the love and support from my family. Words cannot express how grateful I am for all that my parents have provided me throughout my journey. I could not be where I am today without them. Thank you to my siblings, Katie and Brad, for the laughs along the way (and for helping me learn all of the shortcuts on Adobe Premiere Pro). Lastly, I

would like to thank Andrew for always being my biggest fan and believing in me from the beginning.

Table of Contents

List of Figures

List of Tables

List of Symbols

Symbols

c_p	specific heat
D	burner diameter
Δh_c	heat of combustion per mass of fuel
$\dot{m}''$	fuel mass flux, or burning rate
$\dot{m}$	surface mass flow rate
p	pressure
$\dot{q}''$	heat flux
r	radius
R	burner radius
R^*	offset radius
t	time
T	temperature
u	velocity
h_f	flame height

Greek Symbols

μ	viscosity
ρ	density

Subscripts

F	fuel
fl	flame
$O2$	oxygen
Ext	extinction
Osc	oscillation

Chapter 1: Introduction

1.1 Motivation

As the interest in space exploration efforts continue to grow, there is also a growing need to understand the associated risks and potential hazards that are involved. Specifically, the risks and hazards caused by fire in microgravity is a major concern within spacecraft. This is especially important as it concerns sending humans into space. There is a significant amount of research on fire in normal gravity situations. Fire in microgravity has been observed to be different from fire behavior in normal gravity, and research on the subject is still relatively new.

Research regarding the behavior of fire in microgravity increased following a fire incident on the Russian spacecraft Mir in February 1997 [1]. The sustained fire in this incident revealed that there is a prominent need to care about fire safety and understand fire dynamics in microgravity.

Material flammability in space is assessed through a series of testing methods designed by NASA [2]. The BRE project assesses the comprehensiveness of some of these methods. For example, NASA's Test 1 determines the flammability of materials through a pass-fail flame spread test in normal gravity conditions [2], which is insufficient for microgravity purposes [3].

The Burning Rate Emulator (BRE) project is one of five projects currently included in NASA's Advanced Combustion via Microgravity Experiments (ACME), and it specifically focuses on the improvement of fire safety and prevention within spacecraft [4]. The main objective of the project is to improve the fundamental understanding of the flammability of materials, such as the conditions necessary for sustained combustion and extinction behavior [4].

1.2 Literature Review

1.2.1 Flame Extinction

A study on the extinction of small-scale fires using an emulating gas burner was performed by Lundstrom et al [5]. The mechanisms for ignition and extinction were explored with mixtures of methane and propane diluted with nitrogen using a 25 mm BRE burner in normal gravity conditions. The study analyzed the minimum critical mass flux and an associated critical energy flux as criteria for flame ignition and extinction. The critical mass flux criterion changes with the effective heat of combustion of the fuel [5].

In another study, Plathner et al. [6] used gas burners with diameters of 25 mm, 50 mm, and 100 mm to emulate extinction for liquid pools and horizontal solids. Similar to the previous study, extinction was defined as the mass flux at which the flame extinguishes within 5 seconds, when the fuel flow rate to the burner is stepwise decreased [6]. This definition is based on the fire point definition in the Cleveland open cup test [6]. Extinction was obtained by stepwise decreasing the fuel flow rate until the flame went out. The burners emulated the key combustion kinetic properties to governing extinction. This study plots the critical mass flux at extinction for a range of heats of combustion that represents a large variety of solid and liquid fuels. Theory suggests that the heat of combustion and dimensionless mass flux lambda – which includes the critical mass flux, diameter through the heat transfer coefficient, and air properties – are the two important variables for predicting if extinction will occur [6].

These two studies show that the BRE burners provide a simple and more accurate way to emulate extinction conditions compared to standard tests for condensed-phase materials [5],[6].

1.2.2 BRE Development

There have been three designs of BRE burners, the first (BRE 1) was developed by Bustamante. The design had an axisymmetric pyrolysis area with a diameter of 50 mm, and consisted of a perforated brass plate as its surface with hole diameter of 10 mm and 45% open area [7]. This burner was used to emulate methanol, heptane, polymethylmethacrylate (PMMA) and polyoxymethylene (POM) in normal gravity conditions in 2014. These fuels were successfully emulated using propylene, ethylene, and methane diluted with nitrogen [8]. A 25 mm burner was also used in a quiescent chamber to perform microgravity tests in the NASA Glenn 5 s drop facility [8].

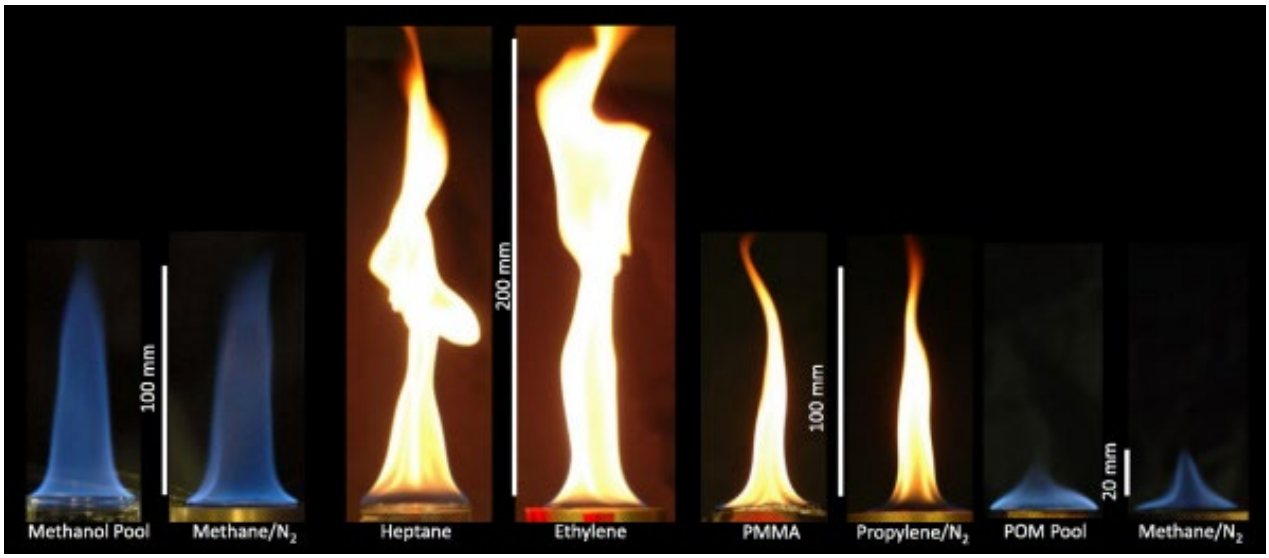

Figure 1.1. Comparison of normal gravity flames of condensed fuels to the 50 mm BRE 1 emulations [8].

The BRE 2 burner was designed by Kim, with the goal to obtain better heat flux measurements and distribution on the surface of the burner [9]. Instead of the brass screen from BRE 1, BRE 2 introduced a thick, porous copper plate to be used as a calorimeter. Thermocouples were embedded into the burner surface, and heat transfer analysis was used to determine the average heat flux to the burner surface [9]. In order to minimize the heat transfer from the copper

plate to the burner body, a stainless-steel body and base plate were used [9]. Tests were performed with the 25 mm and 50 mm BRE 2 burners at NASA Glenn's Zero Gravity Facility with methane, ethylene and nitrogen-diluted ethylene in 2016 [10].

The spaceflight burners (BRE 3) were designed by Markan [3]. The design is similar to that of the BRE 2 burners, but the outer wall is insulated [3]. These burners were used to perform tests on board the International Space Station (ISS) to study flames in microgravity from 2019 to early 2021. The design is discussed in detail within the Description of Experiments chapter.

1.2.3 Emulation

Previous studies of pool fire emulation using gaseous fuels have paved the way to the research performed in present day regarding emulation. These studies were initiated by Corlett [11-13], de Ris et al. [14 -15], and Kim et al. [16]. Corlett performed studies involving the use of gaseous fuels to emulate pool fires to analyze the mechanisms that govern heat transfer [12]. De Ris et al. developed a large-scale burner with a sintered metal surface that used gaseous fuels to examine turbulent flames and radiation effects in normal gravity conditions [15]. The burning conditions of various condensed fuels were correlated to the fuels used by the sintered burner through the Spalding B number – a key factor in controlling the burning rate of condensed fuels. It was also found that emulation of a wide range of solids and liquids could be achieved by varying fuel composition and flow rate to match the Spalding B number or heat of gasification [15]. Kim et al. [16] estimated burning parameters of fuels by studying cylindrical fuel surfaces in inclined, horizontal, and vertical orientations. It was found that both geometric and chemical effects govern laminar burning rates. These studies proved that condensed fuel emulation was possible.

1.2.4 Fire Safety in Space

In February of 1997, a fire ignited in the solid fuel oxygen generator on the Space Station Mir, putting six crew members in danger [1]. Due to increased occupancy on Mir, crew members activated the solid fuel oxygen generator to increase the oxygen supply. The generator operated by burning lithium perchlorate canisters – this reaction produced the oxygen supply needed for the crew members [17]. While replacing the cartridge in the generator, flames large enough to inhibit access to an escape capsule erupted from the generator. Roughly two years after the incident, NASA scientists found that the presence of hydrocarbons in the Lithium Perchlorate canister increased the risk [17]. Later Russian investigators found that just four square centimeters of a latex glove was enough the reproduce the fire [17]. This incident aboard the Mir emphasized the importance of safety procedures and revealed the need to have a better understanding of fire in microgravity conditions.

NASA has established tests to evaluate the flammability of materials in spacecraft. NASA's Upward Flame Propagation Test (Test 1) is a pass-fail test that measures the flame propagation across a sample material in normal gravity conditions [2]. The objective of Test 1 is to determine if a material will self-extinguish in quickly enough to not allow for ignition of adjacent materials when exposed to a standard ignition source [2]. NASA's Test 2 assesses the heat release rate and dynamic smoke production rate of materials by providing an external heat flux by a cone calorimeter and measures the time to ignition of the material [18]. Test 2 provides supplemental information to the results obtained in Test 1.

Although these methods offer some insight into the flammability of the tested materials, they provide an insufficient understanding of diffusion flames in microgravity conditions [19]. Certain phenomena that is present with microgravity flames cannot be addressed with these tests due to the presence of buoyancy in normal gravity conditions [20]. The BRE testing can improve

the understanding a material flammability in microgravity and offer a more well-rounded safety protocol within spacecraft.

1.2.5 Extinction Mechanisms

There is a variety of mechanisms associated with the extinguishment of diffusion flames. Examples include aerodynamic quenching, thermal quenching, and dilution quenching [21]. Aerodynamic quenching occurs when the flame becomes weak due to a critical decrease in the flame residence time by flow-induced disruptions. For thermal quenching to occur, the flame must be weakened by heat losses such as convective or radiant cooling. Dilution quenching occurs when the flame is weakened by composition changes regarding the fuel or oxidizer [21]. For the flames emulated by the Burning Rate Emulator, the observed extinction mechanism is thermal quenching due to radiant cooling. A flame criterion that can explain this phenomenon is known as the Damköhler number (Da), which is defined as the ratio of the characteristic fuel and oxidizer mixing time divided by the characteristic chemical time [21-22].

$$Da \equiv \frac{Characteristic\ Mixing\ Time}{Characterisitic\ Chemical\ Time} = \frac{\tau_{mixing}}{\tau_{chemical}}$$

Extinction is predicted to occur when Da is low – when the fuel and oxidizer mixing time is smaller than the chemical time. From theoretical analysis, it is seen that the characteristic mixing time scales inversely with flame stretch, which is known as the stoichiometric value of the scalar dissipation rate, χ_{st} [21-22]. The scalar dissipation rate is a measure of the fuel and oxidizer mixing rate at the location of the flame. Theoretical analysis also shows that the characteristic chemical time scales like the exponential of the activation temperature divided by the flame temperature [21-22]. Therefore, Da is a function of both flame stretch and flame temperature. The extinction limit associated with thermal quenching, which is exhibited with microgravity flames, is reached when Da is low due to low temperature conditions.

The two types of flame extinction are kinetic and radiative extinction [23]. Short residence times and high strain rates are observed with kinetic extinction. Kinetic (i.e, diffusive) extinction is often observed experimentally in normal gravity conditions, while flames in microgravity are seen to extinguish radiatively [23]. Radiative extinction occurs at low strain rates with longer residence times, which is seen in microgravity flames because the lack of buoyant flow inhibits the straining of the flow field [23].

1.3 Objectives and Preview of Research

This study was performed to improve the understanding of flames in microgravity by measuring and analyzing the oscillation and extinction times of flames emulated using the 25 mm and 50 mm BRE burners on board the International Space Station. The relationships between these measured times and various experimental parameters along with flame characteristics are explored to determine what conditions produce longer lasting – meaning potentially more dangerous – flames. These parameters and flame characteristics include oxygen mole fraction, fuel mole fraction, and fuel mass flow rate, flame height, and heat of gasification.

Chapter 2 discusses the experimental set up of the BRE burners on board the ISS, as well as the design parameters used for testing and the procedures used for data collection. Chapter 3 presents the results from this study and shows the trends that were discovered. A theoretical model for extinction time is also presented in Chapter 3. Chapter 4 offers a set of conclusions based on the findings and provides recommendations for future research.

Chapter 2: Description of Experiments

2.1 BRE Burner Setup

Two BRE burners with diameters of 25 mm and 50 mm are used on the International Space Station (ISS) for these tests. The surface of the burners consists of a perforated copper plate containing 125 holes. Each hole has a diameter of 1.2 mm [24]. The sidewalls of the burner are made of 1 mm thick 304 stainless steel [10]. The copper at the surface acts a as calorimeter that measures the total average heat flux over the burner; it is designed to have a uniform surface temperature. As a result of the edges of the burners being exposed to the flame, the measurements of the heat flux over the burner are uncertain. The copper burner top is painted with Rustoleum High Heat Primer and Rustoleum High Heat Paint. The Rustoleum paint has an absorptivity of 0.91 and an emissivity of 1 [25].

A ceramic flow straightener is used to ensure that there is a uniform fuel flux across the burner surface [24]. Two Medtherm heat flux sensors and thermocouples are located at the burner surface. The heat flux measurements are taken at the center of the burner and at the radius (R*).

A schematic of the 50 mm burner is shown in Figure 2.1 below, followed by Figure 2.2 which depicts an image of the 25 mm with the igniter in place on the ISS, and an illustration of the burner in Figure 2.3.

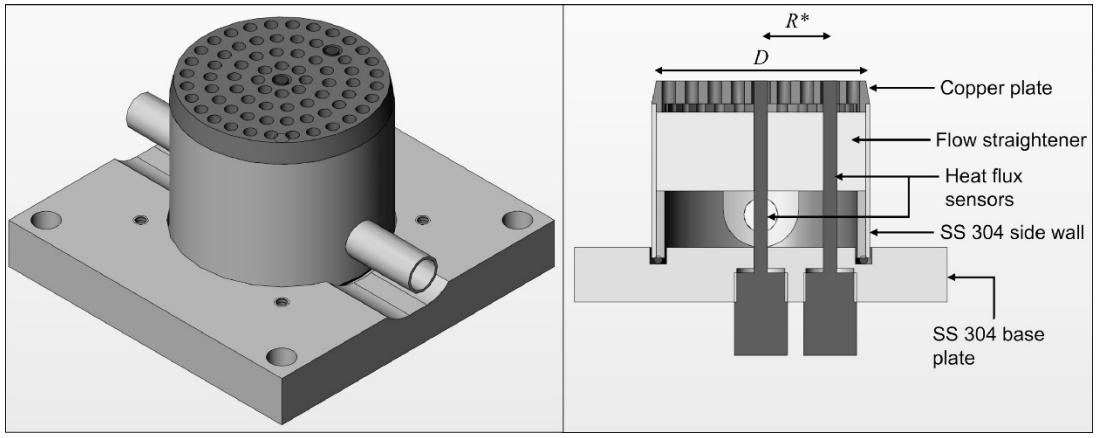

Figure 2.1. Schematic of 50 mm BRE burner [10].

Figure 2.2. 25 mm BRE burner with igniter image (taken from operations camera video footage).

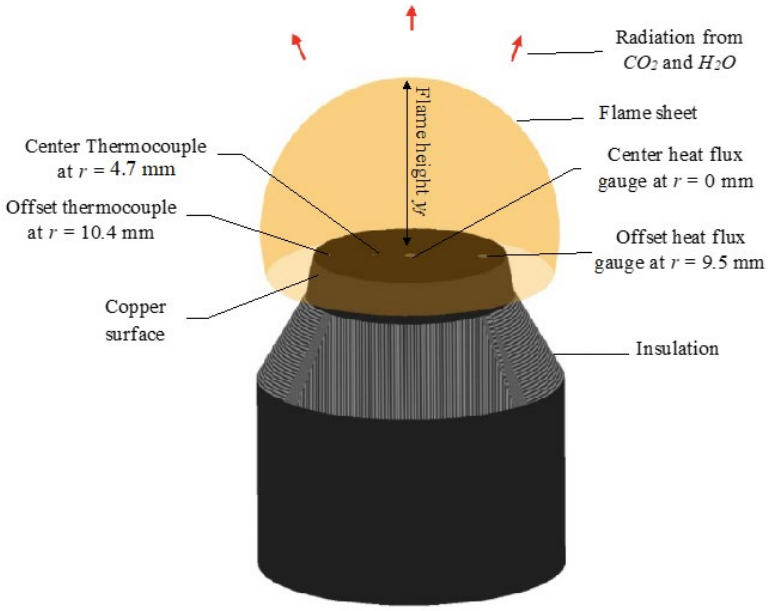

Figure 2.3. Drawing of BRE burner [21].

2.2 Experimental Design

These experiments were performed on the International Space Station (ISS). There were two rounds of testing: Round 1 took place from February to April 2019 and Round 2 took place from August 2020 to January 2021. Round 1 had 59 successful ignitions; of the 59 tests, 30 had instabilities and self-extinguished, while 29 lasted for at least 120 seconds. Round 2 had 137 successful ignitions, with 79 self-extinguished tests. Round 1 testing included ethylene and nitrogen-diluted ethylene (50% mole fraction) as its two fuel mixtures, with heats of combustion of 47.2 and 23.6 kJ/g. The 25 mm BRE burner was the only burner used. Round 2 also tested with nitrogen-diluted ethylene and pure ethylene, but also introduced methane as a third fuel source. The fuel mixtures presented a wide range of effective heats of combustion due to the varying fuel fractions used. Round 2 testing also introduced the 50 mm BRE burner. The additional fuel and burner size allowed for a wider range of measurements to be taken and analyzed.

The burner was installed in a quiescent chamber that was a 100-liter capsule before any of the hardware was installed. The hardware filled approximately 15 liters of the capsule, leaving 85 liters of surrounding volume [24]. The amount of time it takes to deplete the quiescent chamber containing the BRE is dependent on the set parameters of each test such as oxygen mole fraction, fuel mass flow rate, and fuel type. The process for determining the time to deplete the oxygen in the capsule for an ethylene flame test is shown through Equations 2.1-2.4 below.

$$\left[C_2H_4 + \frac{(1 - X_{C2H4})}{X_{C2H4}} N_2\right] + 3\left[O_2 + \frac{(1 - X_{O2})}{X_{O2}} N_2\right] \rightarrow 2CO_2 + 2H_2O + \left(\frac{(1 - X_{C2H4})}{X_{C2H4}} + 3\frac{(1 - X_{O2})}{X_{O2}}\right) N_2 \tag{2.1}$$

$$85L * X_{O2} * \rho_{O2} = Mass\ of\ O_2\ in\ capsule\ (g) \tag{2.2}$$

$$Fuel\ Mass\ Flow\ Rate\ \left(\frac{g}{s}\right) * \left(\frac{3\ mol\ O_2}{1\ mol\ fuel}\right) * \left(\frac{MW_{O2}}{MW_{fuel}}\right) = O_2\ consumed\ from\ Combustion\ \left(\frac{g}{s}\right) \tag{2.3}$$

$$\frac{Mass\ of\ O_2\ in\ capsule\ (g)}{O_2\ consumed\ from\ Combustion\ \left(\frac{g}{s}\right)} = \boldsymbol{Time\ to\ deplete\ O_2(s)} \tag{2.4}$$

To explore the burning effects, the ambient pressure, oxygen concentration, and fuel mass flow rate were changed for each test. These parameters are varied in order to evaluate the flammability of the condensed fuel. Tables 2.1 and 2.2 show the varying design parameters used in Round 1 and Round 2 testing, respectively.

Table 2.1. Design Parameters for Round 1 Tests

Parameter	Units	Conditions Used
BRE Burner Diameter	mm	25
Fuel	-	C_2H_4, Nitrogen-diluted C_2H_4
Fuel Mass Flux $\dot{m}''_{fuel}$	$g/(m^2s)$	1 to 12
Atmospheric Pressure p	bar	0.565, 0.7 and 1
Oxygen mole fraction χ_{O2}	-	0.21, 0.265, 0.34 and 0.4
Pure fuel mole fraction χ_F	-	0.5 and 1

Table 2.2. Design Parameters for Round 2 Tests

Parameter	Units	Conditions Used
BRE Burner Diameter	mm	25 and 50
Fuel	-	C_2H_4, Nitrogen-diluted C_2H_4, CH_4
Fuel Mass Flux $\dot{m}''_{fuel}$	$g/(m^2s)$	1 to 12
Atmospheric Pressure p	bar	0.565, 0.7 and 1
Oxygen mole fraction χ_{O2}	-	0.21, 0.265, 0.34 and 0.4
Pure fuel mole fraction χ_F	-	0.1-1

2.3 Mass Flux

The mass flux of the fuel-nitrogen mixture simulates condensed-phase burning. The volumetric flow rate of the fuel is measured using an HFM-300 Hastings instrument with a maximum flow rate of 0.2 standard liter per minute (slpm) for low mass flux experiments and 0.5 slpm for high mass flux experiments [24]. The mass flow controllers are calibrated using nitrogen. For these tests, the gas conversion factors are 0.606, 0.775, and 0.779 for pure ethylene, diluted

ethylene, and methane, respectively [24]. At the surface of the burner, the mass flux of the fuel is low and similar to those that occur during the burning of condensed fuels [10].

2.4 Flame Radiation

Radiometers from Dexter Research Inc. are used to view the flames from the burner and the burner's surface. They are placed at distances of about 160 and 200 mm away from the burners [24]. The viewing window of these radiometers are made of barium fluoride and argon is used to fill the void volume between the sensing surface and window [24]. NASA calibrated these radiometers using varied temperature and aperture sizes, as well as a black-body radiation source. The total radiation loss by the flame could be estimated from the radiometers, which were used to determine the sensor normal radiant heat flux from the flame and burner.

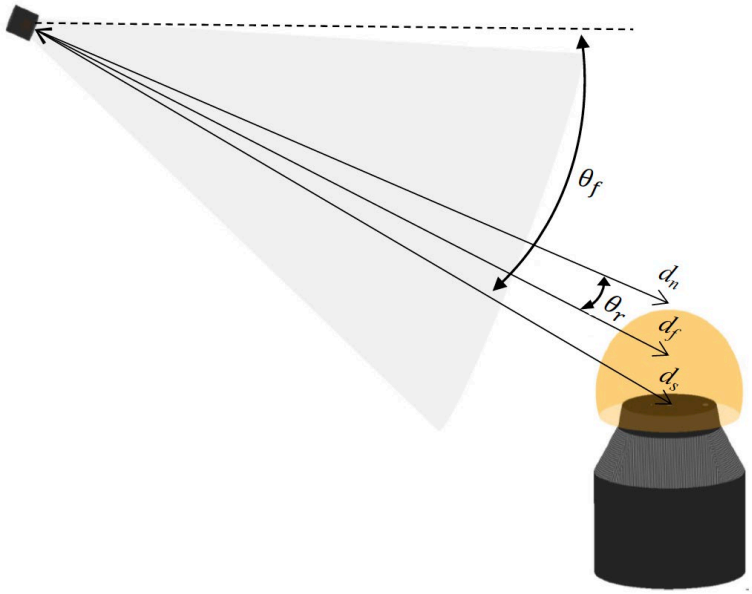

Figure 2.4. Schematic of radiometer setup [21].

2.5 Image and Video Processing

2.5.1 OPS Camera

Videos were recorded by the operations camera (OPS camera) using a frame rate of 30 fps; it was positioned to view the flames through the chamber windows. These videos were edited in

Adobe Premiere Pro to adjust for brightness so that flame destabilization and oscillation could be easily observed. In addition, the adjustment allowed the end time of the flame test—either from self-extinguishment or fuel termination—to be more easily observed. The outline of the burner was traced and drawn in Adobe Illustrator and then imported into the Premiere Pro videos so that the burner position could be visualized for the duration of each test. For the purposes of this study, the tests that resulted in self-extinguishment are analyzed.

2.5.2 ACME Camera

Another camera used to capture still images of the tests was the ACME camera. The ACME camera images are produced in the HOBJ format, which are converted to colored images by using the OMA2 image processing software. The detailed process of converting the HOBJ images into viewable JPEGS and TIFFS using OMA2, as well as the process of making the images into image sequence videos, is described in the Appendix.

2.6 Data Collection

2.6.1 Measuring Oscillation and Extinction Times

A time code was placed on each video so that the time to oscillation and the extinction time of each flame could be observed in relation to the time of ignition; time of ignition occurred at 0 seconds according to the time code. These videos from the OPS camera were used to document the oscillation and extinction times by taking note of the frame when each flame began to oscillate and when the flame went extinct. This was done for all of Round 1 and Round 2 tests. An image sequence of an ethylene flame test is shown in Figure 2.5 below.

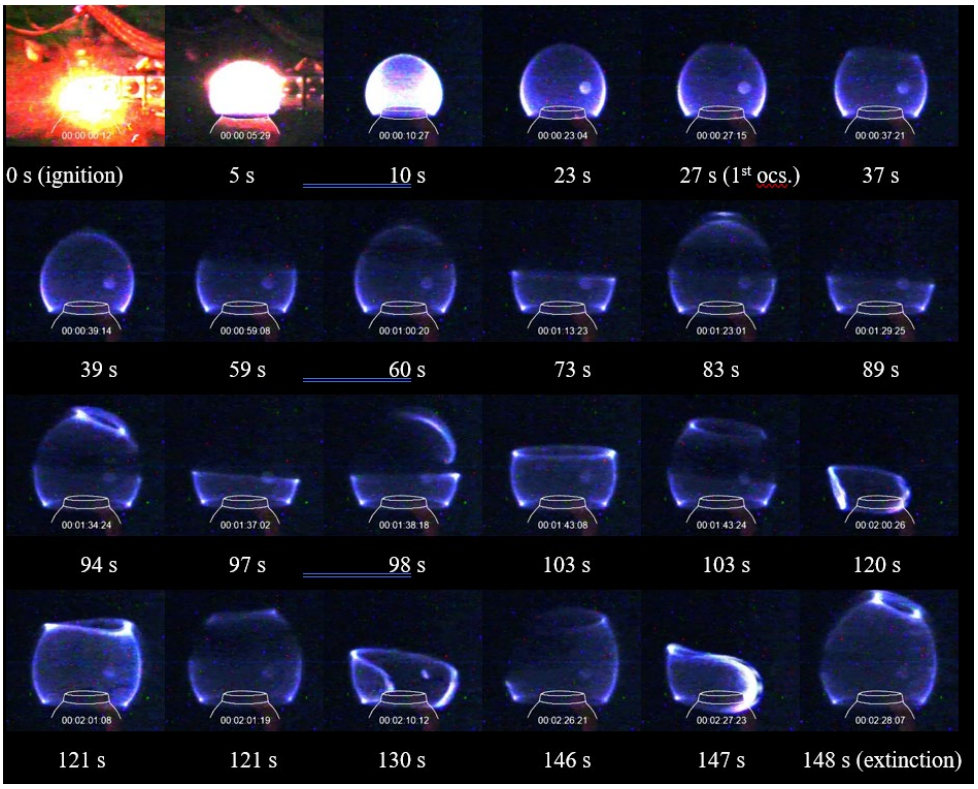

Figure 2.5. Image sequence of ethylene flame from ignition to oscillation to self-extinguishment.

Another method was used to obtain the oscillation onset and flame extinction times for each flame by analyzing Photomultiplier Tube (PMT) data with respect to time. The PMT with OH* filter assembly represents flame luminosity and illustrates the flame behavior throughout the duration of the test [24]. This method was more rigorous procedure that offered more accurate results for measuring the extinction times and was used to determine the results of this study. Data from the mass flow controller was also used to determine which tests resulted in self-extinguishment or fuel termination. Figures 2.6 and 2.7 below show examples of PMT and mass flow plots used to analyze the behavior of an ethylene flame.

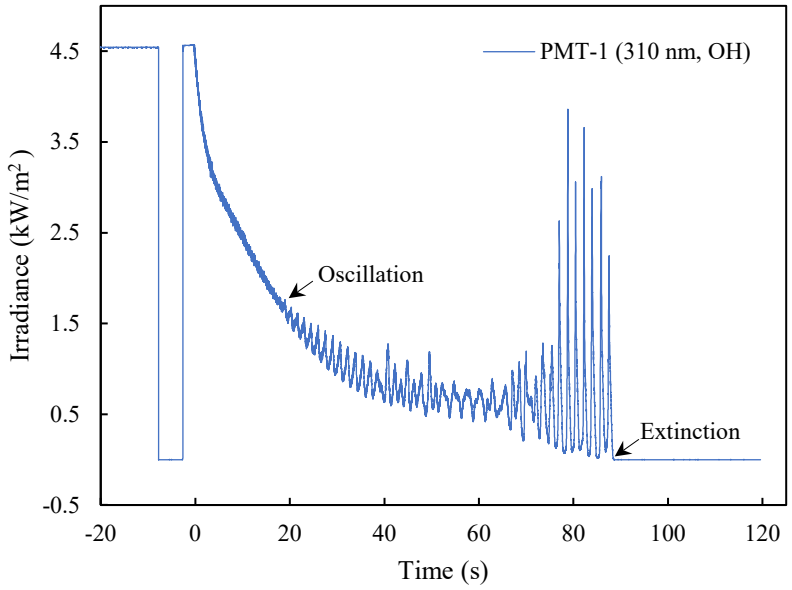

Figure 2.6. PMT plot of an ethylene flame showing the time of oscillation onset and extinction.

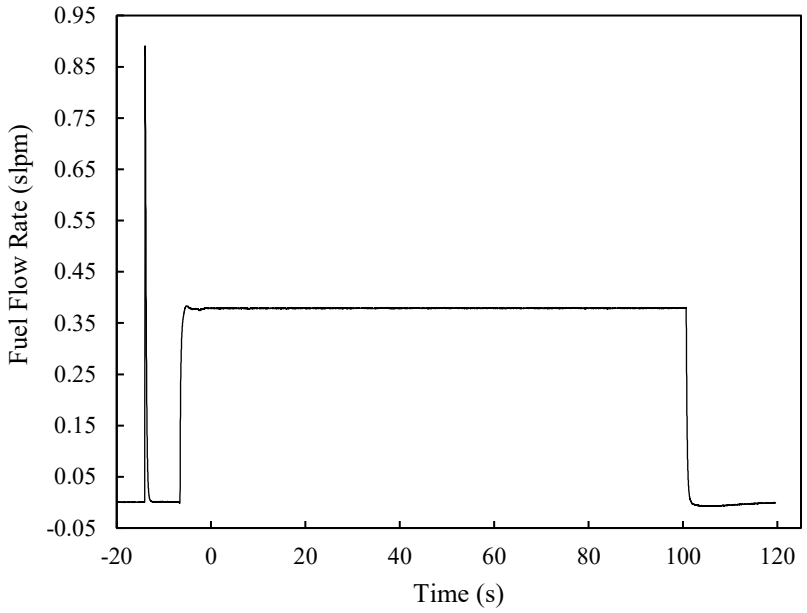

Figure 2.7. Fuel mass flow rate from mass flow controller as a function of time. The fuel was cut off after the flame oscillations ended shown in Figure 2.6, indicating that the flame self-extinguished.

2.6.2 Measuring Flame Height and Radius

Snapshots from the OPS camera videos were extracted from Adobe Premiere Pro and used to measure the flame height of each test. Snapshots were taken of the frame directly before the flame started to oscillate. These snapshots were then imported into FIJI ImageJ, where the flame height and diameter were measured by length in pixels and burner diameter. The height was measured from the center of the burner to the top of the flame sheet. The flame diameter was measured across the bottom of the flame closest to the burner surface. Figure 2.8 below shows an example of a flame height and diameter measurement on ImageJ. Using the known diameter of the burner surface in millimeters (either 50 mm or 25 mm), the actual flame height and radius could be calculated in millimeters. An uncertainty of +/- 5% was assumed for these measurements.

Images from the ACME camera were used to measure the flame heights and radiuses for 10 of the tests at the end of Round 2 because the full view of the flame was obstructed by a temperature fiber bracket in some of the OPS video footage.

Figure 2.8 Sample image showing how the pixel lengths of a flame height and diameter were determined on ImageJ.

Chapter 3: Results

The results consist of trends between extinction time and various experimental parameters as well as flame characteristics. The measured oscillation onset and extinction times were plotted against parameters such as oxygen mole fraction, fuel mole fraction, and fuel mass flow rate. The times were also plotted against flame characteristics such as flame height and heat of gasification. These trends are depicted in the following sections. An uncertainty of +/- 5% was assumed for the time measurements as well as the flame height measurements. To make some of the plots easily viewable, error bars were applied to only one data point, but it is assumed that the rest of the data contains the same amount of uncertainty.

3.1 Oxygen Mole Fraction and Extinction Time Relationship

Figures 3.1 and 3.2 below show the relationship between the measured extinction time and the oxygen mole fraction that was set for each test for C_2H_4 and CH_4, respectively. The oxygen mole fractions ranged from 0.21 to 0.4. Generally, higher oxygen molar concentrations produced flames with higher extinction times.

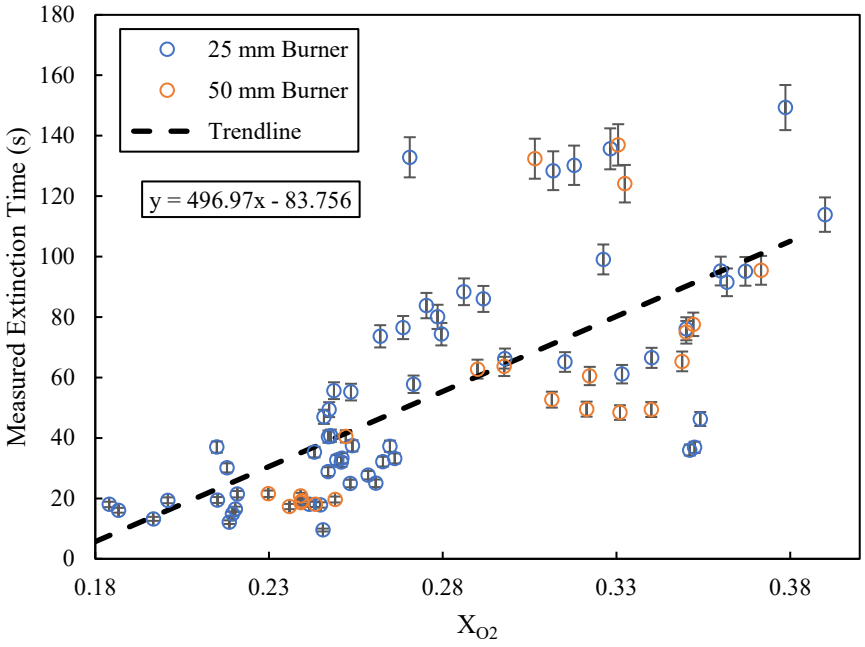

Figure 3.1. Extinction time as a function of molar oxygen fraction with C_2H_4 as the fuel, including both the 25 mm and 50 mm burner data.

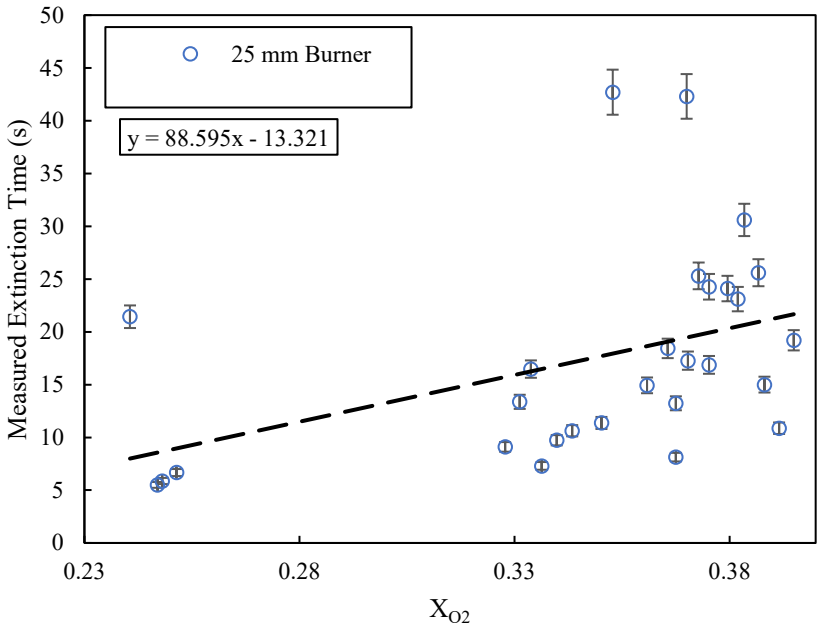

Figure 3.2. Extinction time as a function of molar oxygen fraction with CH_4 as the fuel, using the 25mm burner.

From Figure 3.1, it can be seen that the burner size did not affect the relationship between molar oxygen fraction and flame extinction time – extinction time increased as oxygen mole fraction increased for C_2H_4 using both BRE burners. Figure 3.2 shows this same trend for the tests done with CH_4 as the fuel source using the 25 mm burner, although CH_4 flames generally self-extinguished much sooner than the C_2H_4 flames. The burn time for the C_2H_4 flames ranged from 10 to 150 seconds before self-extinguishment, while the CH_4 burn time ranged from 5 to 43 seconds.

3.2 Fuel Mole Fraction and Oscillation Time Relationship

Figures 3.3 and 3.4 show the relationship between the fuel mole fraction and the time until oscillation. The fuel mole fraction ranged from 0.33 to 1. Due to a few outliers in regard to flame extinction time, the trend was more easily seen with the oscillation onset instead.

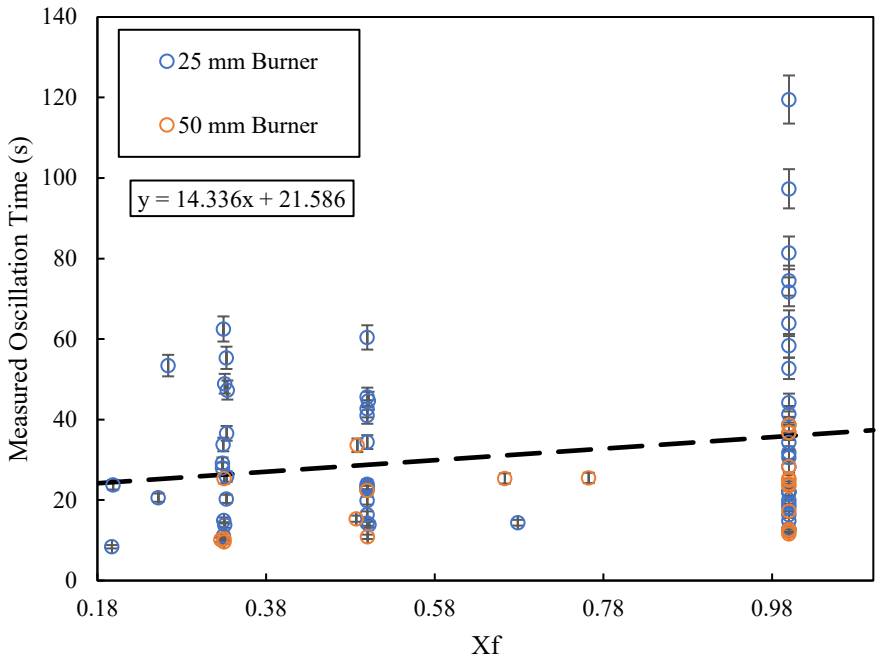

Figure 3.3. Oscillation time as a function of molar fuel fraction with C_2H_4 as the fuel, including both the 25 mm and 50 mm burner data.

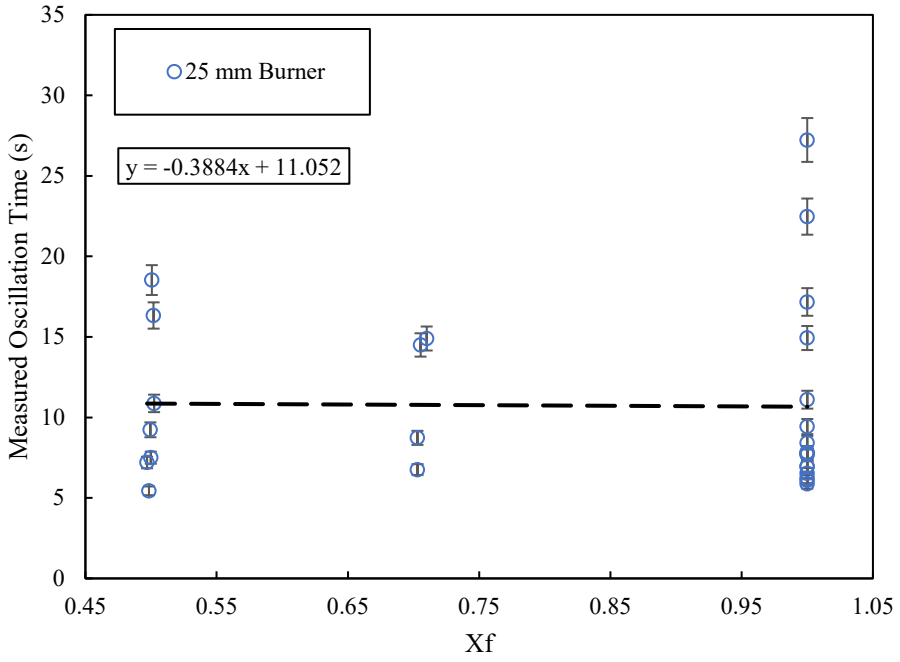

Figure 3.4. Oscillation time as a function of molar fuel fraction with CH_4 as the fuel, using the 25mm burner.

Higher fuel mole fractions produced some flames with longer oscillation times, although this trend is not as clear compared to the relationship with oxygen mole fraction. There are inconsistencies present – some CH_4 tests with a fuel mole fraction of 0.5 produced flames with longer stability than tests with a fuel mole fraction of 0.7, for example. However, for both C_2H_4 and CH_4, the longest stabilities occurred when the fuel mole fraction was 1. Figure 3.3 also shows that tests done with the 25 mm burner generally remained stable for longer than the tests done with the 50 mm burner, suggesting that smaller flames can survive longer than larger flames.

3.3 Fuel Mass Flow Rate and Extinction Time Relationship

It was found that lower fuel mass flow rates resulted in longer-lasting flames for both fuels at varying oxygen and fuel mole fractions. To see the trends, the data needed to be separated by oxygen mole fraction and ambient pressure. Figure 3.5 depicts the results for C_2H_4 at 14.7 psia

with an oxygen mole fraction of 0.21, while Figure 3.6 depicts the results for CH_4 at 14.7 psia with an oxygen mole fraction of 0.4. Each of these plots show both the oscillation and extinction times and present tests with varying fuel mole fractions. Plots consisting of the remaining combinations of oxygen mole fraction and pressure for the two fuels can be found in the Appendix.

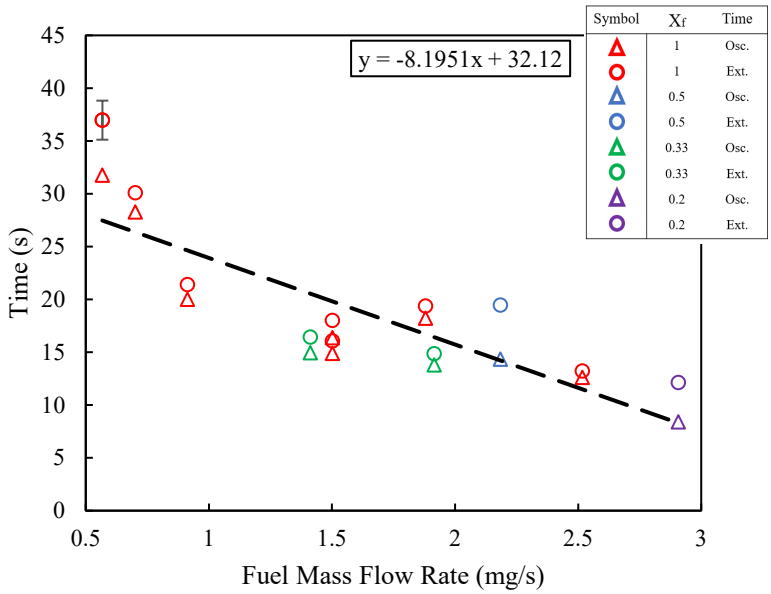

Figure 3.5. Extinction and oscillation time relationship with fuel mass flow rate for C_2H_4 with an ambient pressure of 14.7 psia and oxygen mole fraction of 0.21.

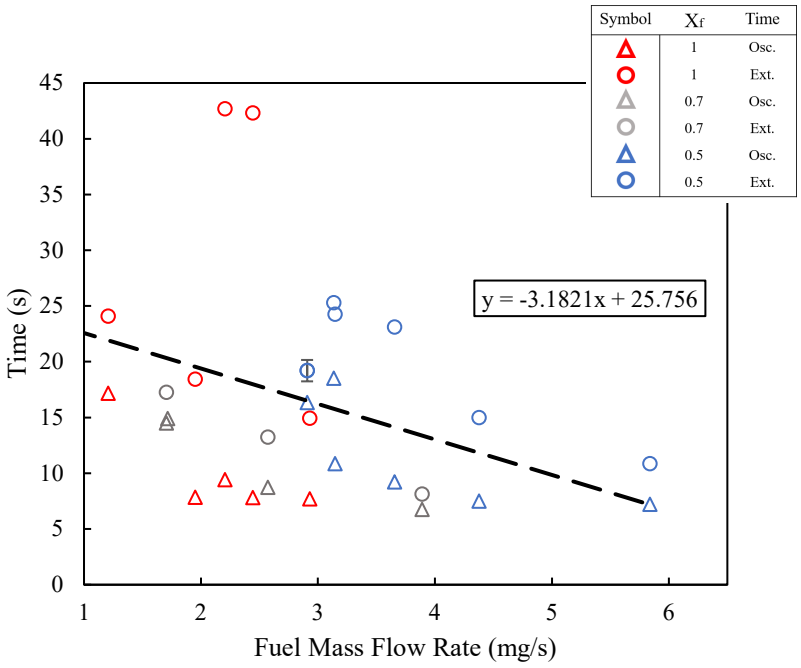

Figure 3.6. Extinction and oscillation time relationship with fuel mass flow rate for CH_4 with an ambient pressure of 14.7 psia and oxygen mole fraction of 0.4.

Both Figure 3.5 and 3.6 show that extinction time and fuel mass flow rate generally have an inverse linear relationship in which the time until extinction decreases as the fuel mass flow rate increases for various fuel mole fractions. This presents the idea that smaller mass fluxes produce longer-lasting flames, which means these flames could be potentially more hazardous on spacecraft because the longer burn time increases the likelihood of the flame spreading to adjacent materials.

3.4 Flame Height and Extinction Time Relationship

The relationship between flame height and extinction time resulted in similar trends to the trends shown in Section 3.3. Smaller flames tended to stay stable and last longer than larger flames. Figures 3.7 and 3.8 show this relationship for C_2H_4 at 8.2 psia with an oxygen mole fraction of

0.34 and CH_4 at 14.7 psia with an oxygen mole fraction of 0.4, respectively. The remaining flame height versus extinction time plots are shown in the Appendix.

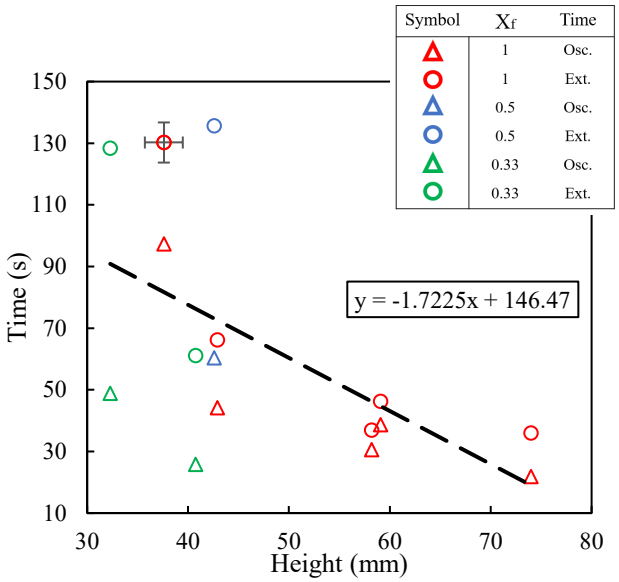

Figure 3.7. Extinction and oscillation time relationship with flame height for C_2H_4 with an ambient pressure of 8.2 psia and oxygen mole fraction of 0.34.

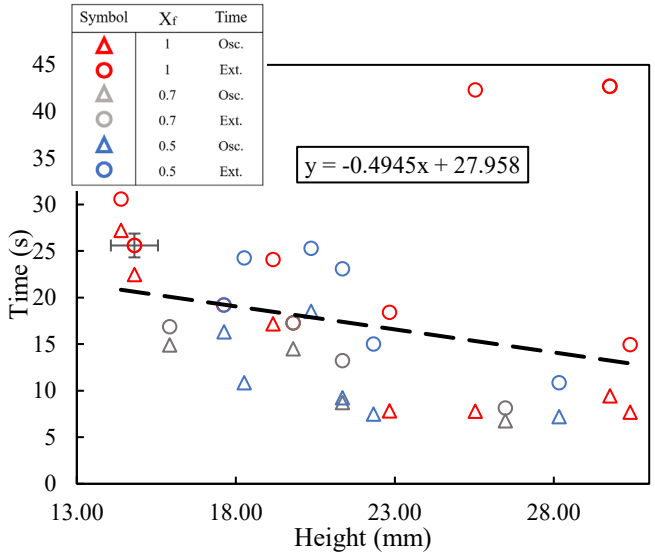

Figure 3.8. Extinction and oscillation time relationship with flame height rate for CH_4 with an ambient pressure of 14.7 psia and oxygen mole fraction of 0.4.

Similar to the relationship between extinction time and fuel mass flux, extinction time and flame height have a negative linear relationship. Despite two outliers within the CH_4 flames, larger flames became unstable and self-extinguished much sooner than smaller flames.

3.5 Heat of Gasification

Extinction and oscillation times were plotted against the heat of gasification values for each flame. Due to the short duration for the majority of the CH_4 tests, condensation on the burner did not evaporate before many of the flames extinguished. Therefore, the data from the heat flux sensors was not reliable and heat of gasification values could not be appropriately calculated. No visible relationship was determined from the reliable data obtained.

3.6 Theoretical Model for Extinction Time

The extinction time relationships found between oxygen mole fraction as well as fuel mass flux offer qualitative results that aid in a better understanding of burning in microgravity. However, relationships could only be seen when the data was separated based on oxygen mole fraction and pressure. A theoretical model was determined that collapses all the time data onto one plot for extinction time as well as oscillation onset using power regression analysis.

The measurements are reasonably correlated by scaling the oscillation onset and extinction times with $X_{O2}^3\ \mathrm{Re}^{-0.5}$, where Re is the jet Reynolds number. Equations 3.1 and 3.2 below show the models determined for extinction time and oscillation onset, respectively.

$$t_{ext} = AX_{O2}^{3.42}Re^{-0.424} \tag{3.1}$$

$$t_{osc} = AX_{O2}^{2.63}Re^{-0.620} \tag{3.2}$$

Where the A coefficient has seconds as its unit and varies based on fuel type and burner diameter. Table 3.1 below show the coefficients for each model.

Table 3.1. Coefficient Values for Extinction Time and Oscillation Onset Models

Model Coefficients (s)		
Fuel	Extinction	Oscillation
C2H4 (25 mm)	5085	1356
C2H4 (50 mm)	3739	660
CH4	601	199

The derivation that illustrates the relationship between the Reynolds number and fuel mass flow rate is shown through Equations 3.3-3.6 below.

$$Re = \frac{\rho_f u d}{\mu} \tag{3.3}$$

ρ is the density of the fuel, u is the velocity at which the fuel is flowing out of the burner holes, d is the characteristic length, which is the burner diameter, and μ is the viscosity of the fuel mixture. The velocity can be calculated by Equation 3.4.

$$u = \frac{\dot{m}}{\rho_f \left(\frac{\pi}{4}\right) d^2} \tag{3.4}$$

Substituting Equation 3.4 into Equation 3.3 results in Equation 3.5.

$$Re = \frac{\dot{m}}{\left(\frac{\pi}{4}\right) \mu d} \tag{3.5}$$

Assuming μ remains constant for the fuel mixture at the specified pressure, it can be seen that the Reynolds number is proportional to the fuel mass flow rate and depends on the burner diameter.

$$Re = \frac{\dot{m}}{d} \tag{3.6}$$

Figures 3.9 and 3.10 below show the correlations between the measured and modeled times.

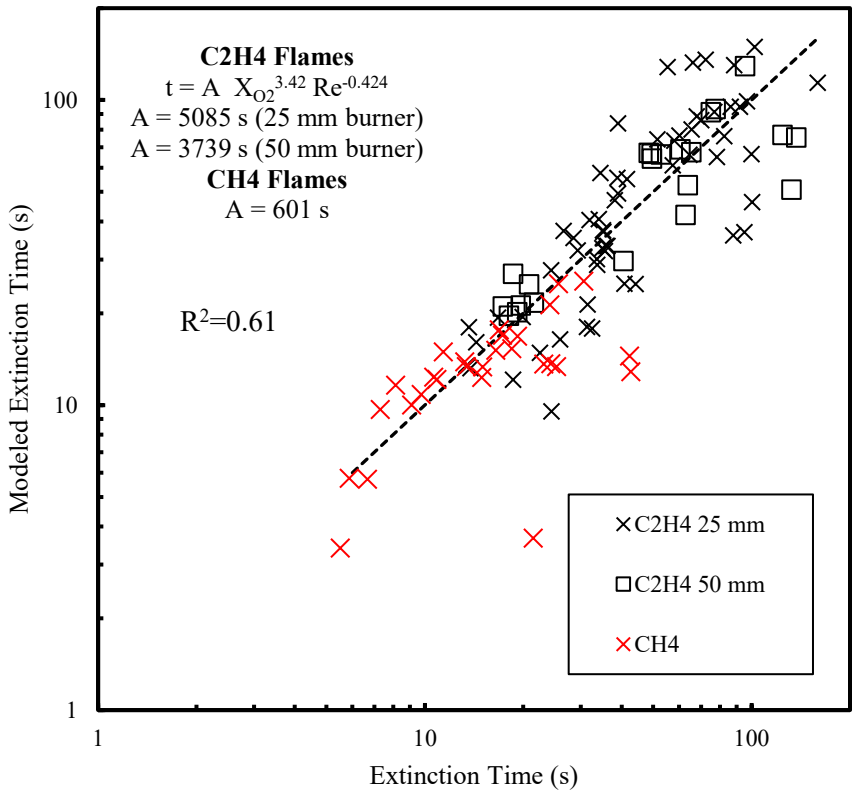

Figure 3.9. Correlation between measured and modeled extinction times.

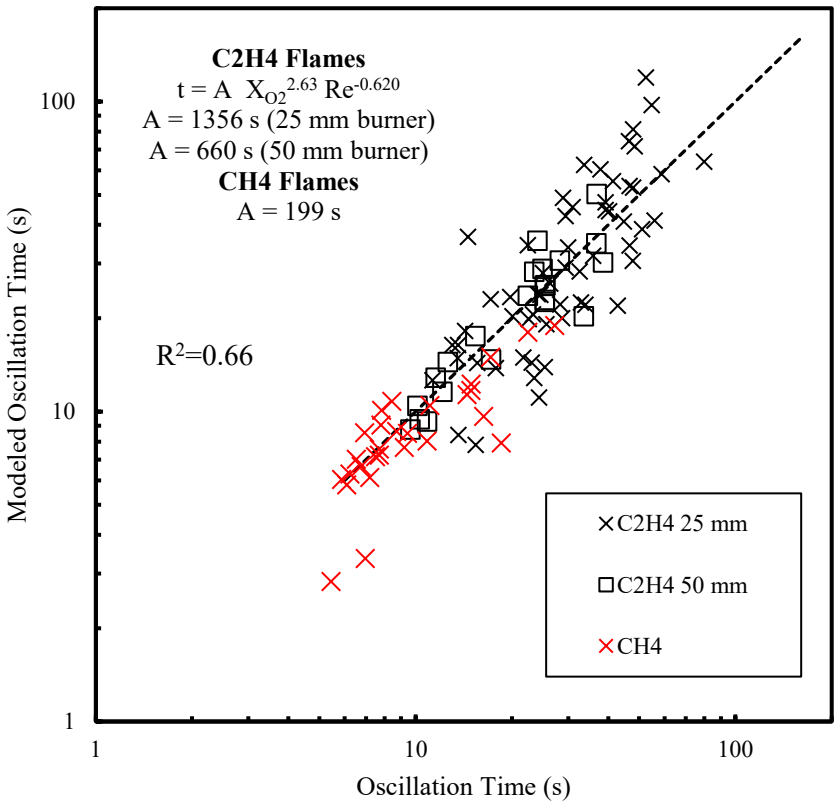

Figure 3.10. Correlation between measured and oscillation onset.

The modeled times correlate reasonably well with the measured times, with an R^2 value of 0.61 and 0.66 for extinction time and oscillation onset, respectively. These models quantify longer burning at higher oxygen concentrations and lower mass flow rates, which could potentially be used to predict the burn time of a flame by knowing the oxygen conditions and mass flow, independently from the pressure.

Chapter 4: Conclusions and Future Research

4.1 Conclusions

Understanding the hazards caused by fire in microgravity conditions is important, especially as space exploration efforts continue to increase. Emulating condensed fuels with gaseous ethylene and methane diluted with varying amounts of nitrogen with the Burning Rate Emulator offers more of an understanding of material flammability in microgravity and provides information that can improve safety standards within spacecraft.

This research aims to add to the understanding specifically of flame extinction behavior in microgravity. By measuring the oscillation onset and extinction times for the emulated flames, relationships between the extinction times and various experimental parameters were able to be explored. Higher oxygen fractions produced longer-lasting flames, showing that there are significant hazards with the use of enriched oxygen atmospheres in spacecraft. Lower mass flow rates resulted in longer-lasting flames, and flames with smaller flame heights were seen to burn longer than larger flames. These findings suggest that the hazards associated with small fires warrant more consideration.

Based on the qualitative findings, a model was determined to quantitatively show the effect that oxygen mole fraction and fuel mass flow rate have on extinction behavior. The model could be used to predict oscillation onset and extinction time based on a known material and known oxygen environment.

The various parameters used for testing offered a wide range of measurements to be analyzed and related to real life conditions. By varying the fuel mole fraction and fuel mass flow rate, the heats of combustion and gasification could be matched to real materials present within spacecraft; examples include materials such as nylon and PMMA. Varying the oxygen mole fraction and ambient pressure allowed for the effects of burning to be explored in different

atmospheres. Specifically, three of the atmospheres tested were matched to NASA selected atmospheres for humans within space flight – 34% oxygen and 8.2 psia, 26.5% oxygen and 10.2 psia, and 21% oxygen and 14.7 psia [24]. Measuring the oscillation onset and extinction times for flames under these conditions allows for a better overall understanding of fire behavior within spacecraft.

4.2 Future Research

For future research, refinement of the oscillation onset and extinction time models could be done to obtain stronger correlations between measured and modeled times. This study primarily focused on the self-extinguished tests from the BRE burner. Data from tests in which the fuel supply was terminated but still exhibited instabilities could be added to the oscillation onset model. The data from the fuel terminated tests could be added to the model to predict when instabilities and self-extinguishment could have been expected for "steady" flames.

The heat of gasification is a key property in matching the emulated fuels to real materials [24]. Although a correlation between heat of gasification and extinction time was not successfully determined in this study, further analysis is suggested to see if there is a meaningful relationship present. Because of the relatively short durations of the methane flames, condensation effects caused the heat flux readings to be unreliable and heat of gasification values could not be appropriately calculated. Determining a way to account for this effect would help to obtain reliable heat of gasification values for short-duration flames.

The main objective of the Burning Rate Emulator is to increase the understanding of material flammability in microgravity in order to improve safety conditions within spacecraft. Therefore, it is necessary to continue to develop a flammability map that contains as many materials as possible by using the various ISS testing parameters.

Appendix A. Extinction Time and Oscillation Onset Plots

A.1 Oxygen Mole Fraction

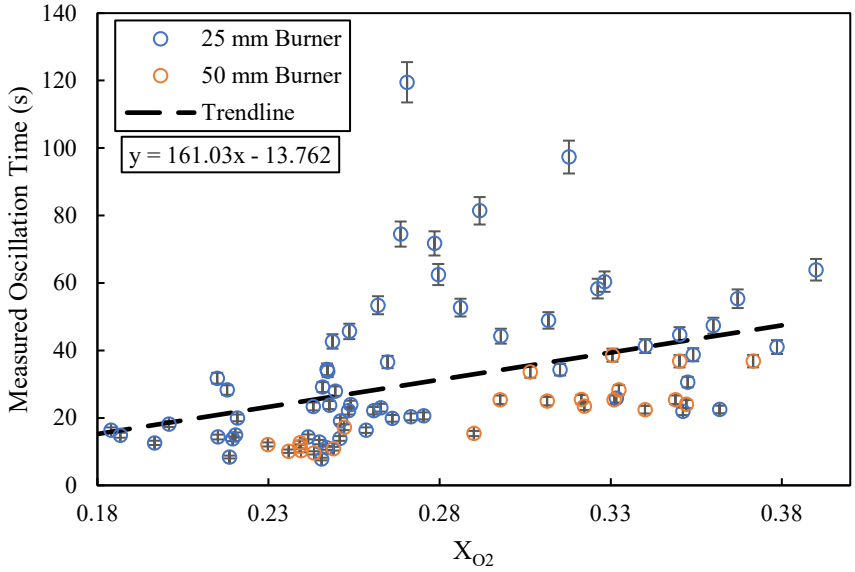

Figure A.1. Oscillation time as a function of molar oxygen fraction with C_2H_4 as the fuel.

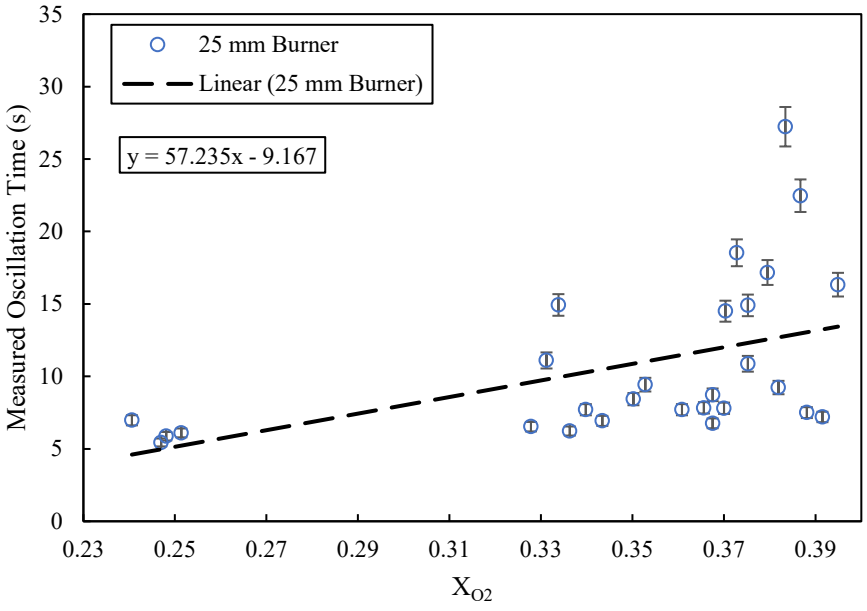

Figure A.2. Oscillation time as a function of molar oxygen fraction with CH_4 as the fuel.

A.2 Fuel Mole Fraction

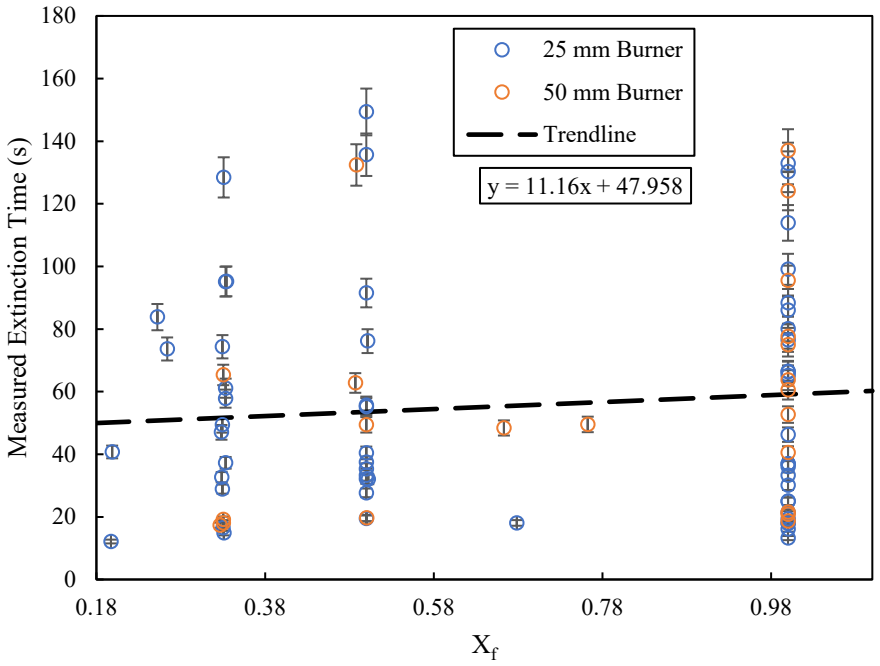

Figure A.3. Extinction time as a function of molar oxygen fraction with C_2H_4 as the fuel.

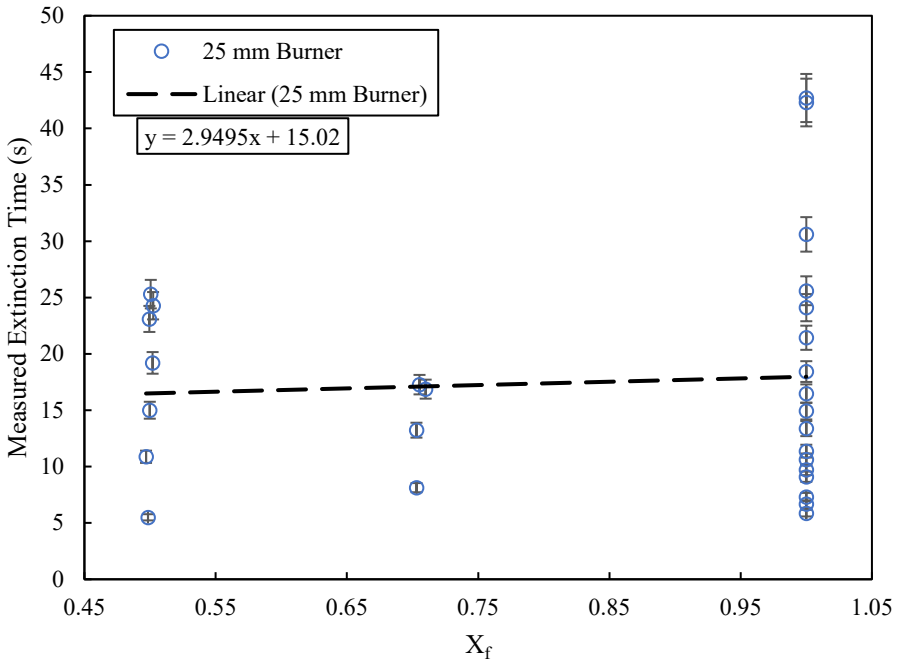

Figure A.4. Extinction time as a function of molar oxygen fraction with CH_4 as the fuel.

A.3 Mass Flow Rate

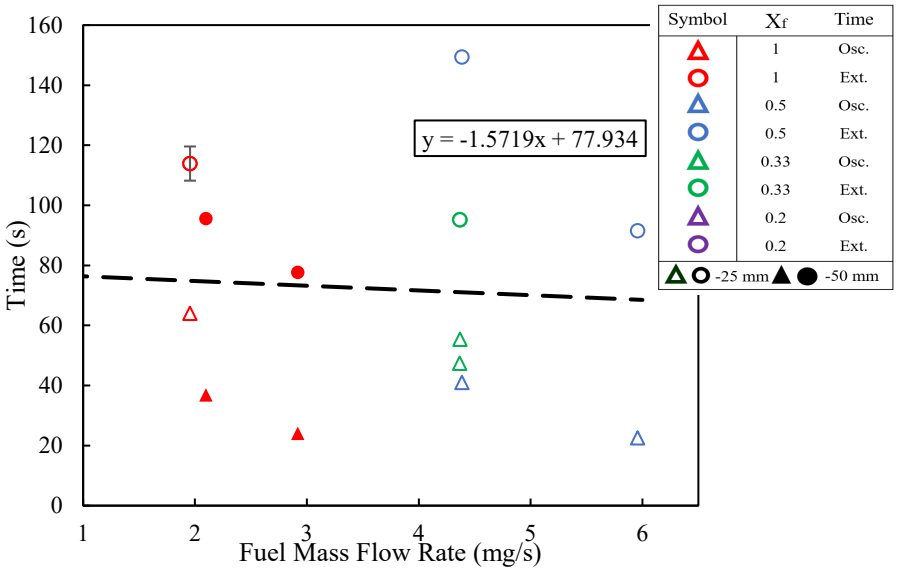

Figure A.5. Extinction and oscillation time relationship with fuel mass flow rate for C_2H_4 with an ambient pressure of 14.7 psia and oxygen mole fraction of 0.4.

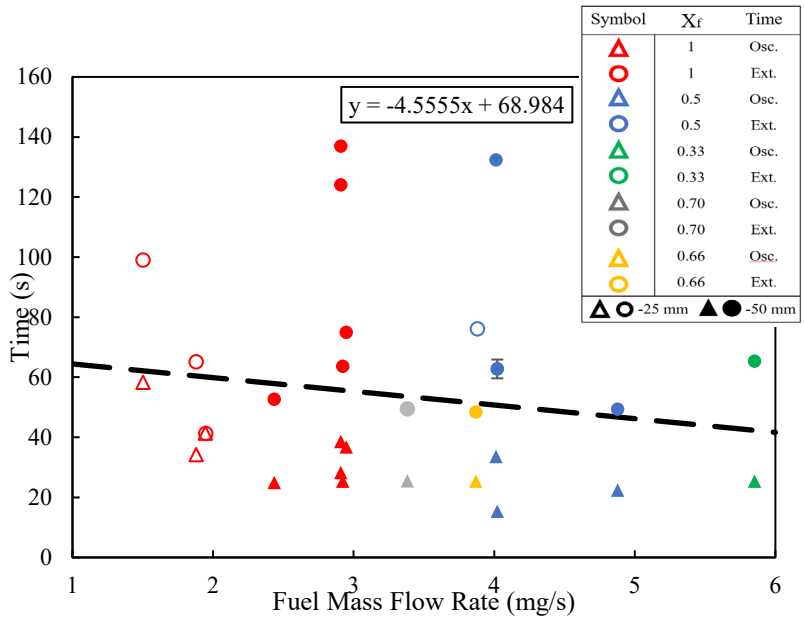

Figure A.6. Extinction and oscillation time relationship with fuel mass flow rate for C_2H_4 with an ambient pressure of 14.7 psia and oxygen mole fraction of 0.35.

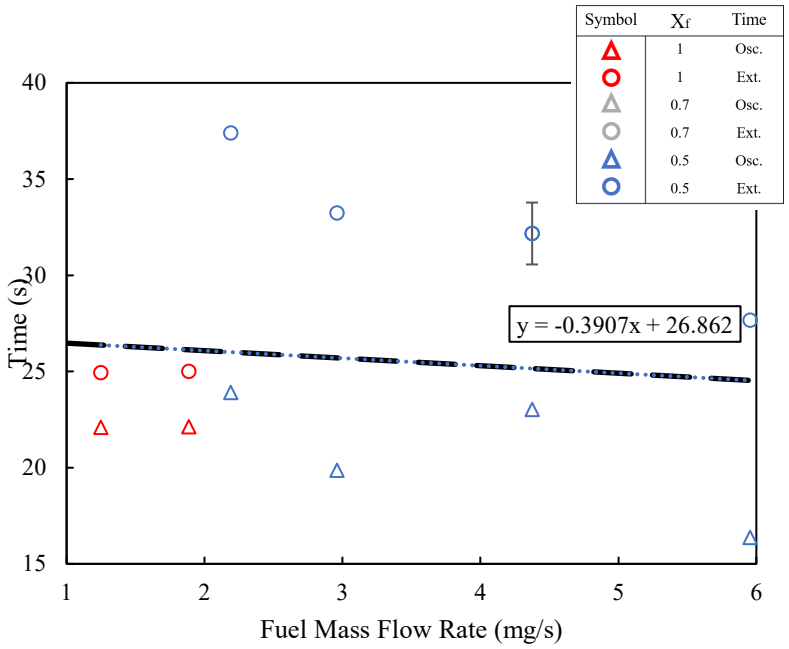

Figure A.7. Extinction and oscillation time relationship with fuel mass flow rate for C_2H_4 with an ambient pressure of 14.7 psia and oxygen mole fraction of 0.27.

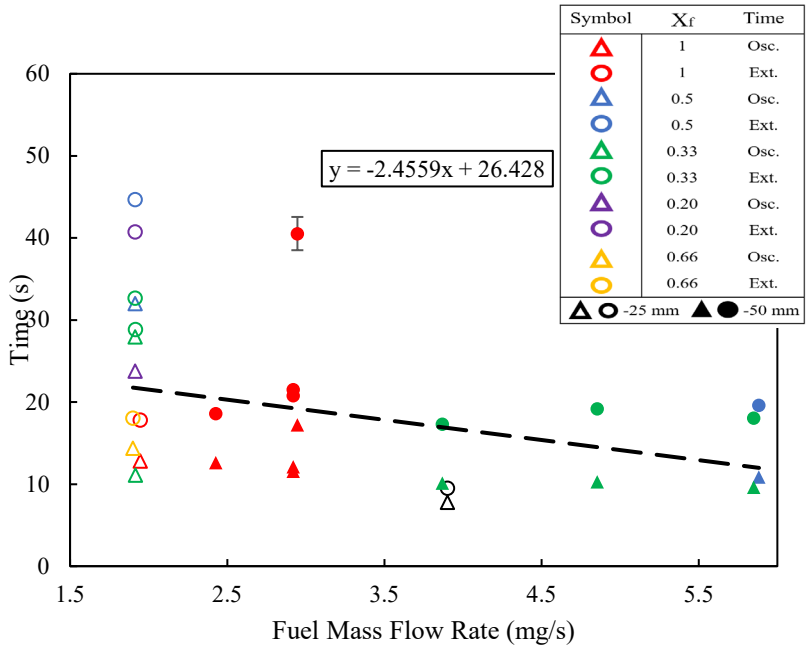

Figure A.8. Extinction and oscillation time relationship with fuel mass flow rate for C_2H_4 with an ambient pressure of 14.7 psia and oxygen mole fraction of 0.25.

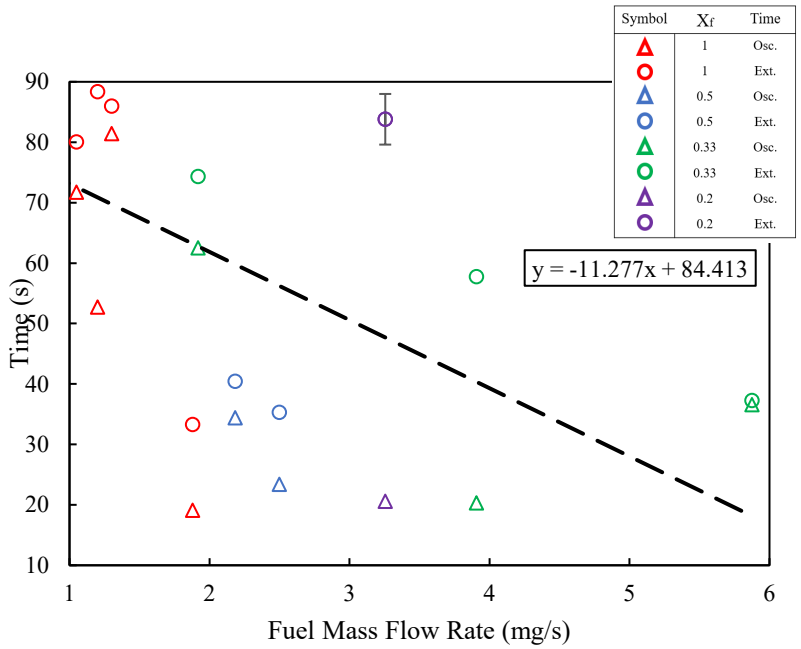

Figure A.9. Extinction and oscillation time relationship with fuel mass flow rate for C_2H_4 with an ambient pressure of 10.2 psia and oxygen mole fraction of 0.27.

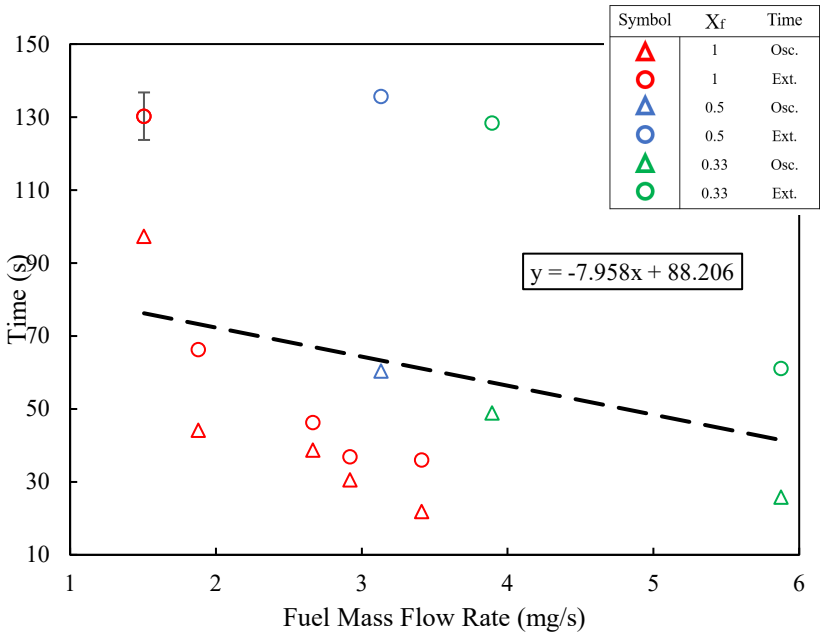

Figure A.10. Extinction and oscillation time relationship with fuel mass flow rate for C_2H_4 with an ambient pressure of 8.2 psia and oxygen mole fraction of 0.34.

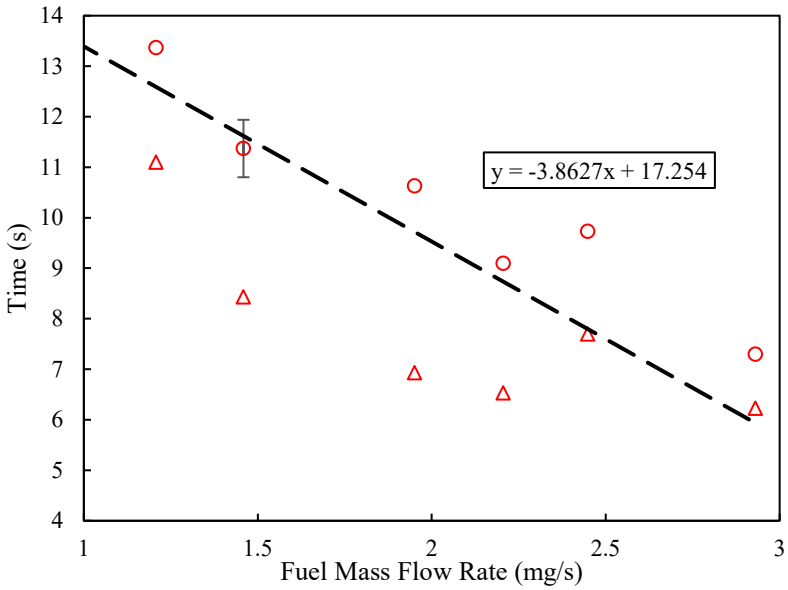

Figure A.11. Extinction and oscillation time relationship with fuel mass flow rate for CH_4 with an ambient pressure of 14.7 psia and oxygen mole fraction of 0.34 and fuel mole fraction of 1.

A.4 Flame Height

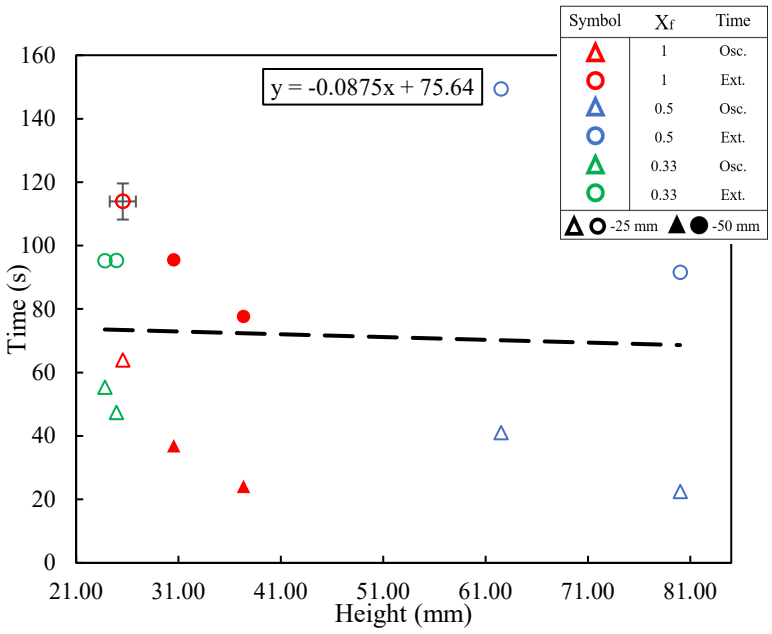

Figure A.12. Extinction and oscillation time relationship with flame height for C_2H_4 with an ambient pressure of 14.7 psia and oxygen mole fraction of 0.4.

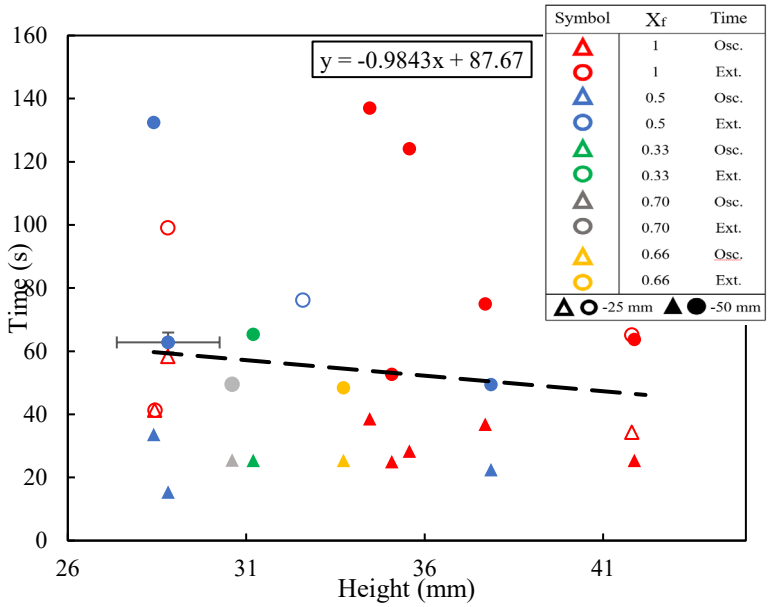

Figure A.13. Extinction and oscillation time relationship with flame height for C_2H_4 with an ambient pressure of 14.7 psia and oxygen mole fraction of 0.35.

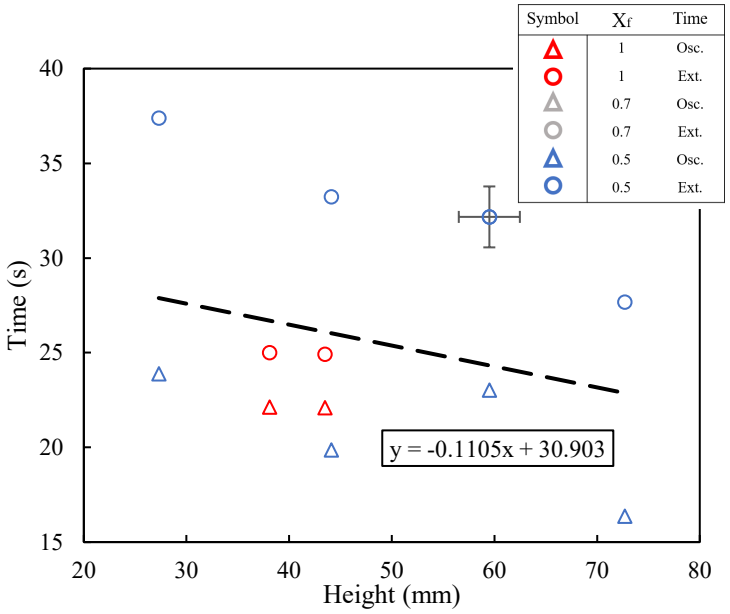

Figure A.14. Extinction and oscillation time relationship with flame height for C_2H_4 with an ambient pressure of 14.7 psia and oxygen mole fraction of 0.27.

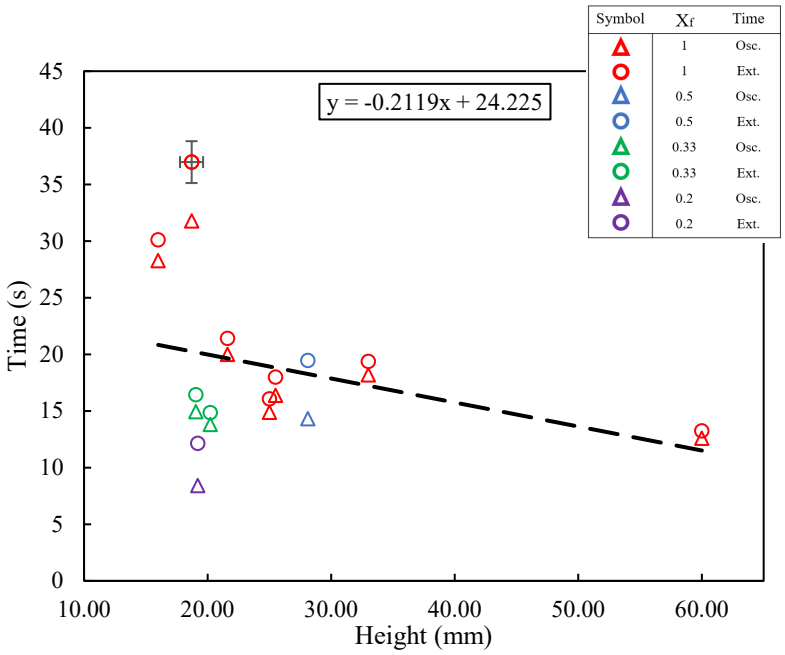

Figure A.15. Extinction and oscillation time relationship with flame height for C_2H_4 with an ambient pressure of 14.7 psia and oxygen mole fraction of 0.21.

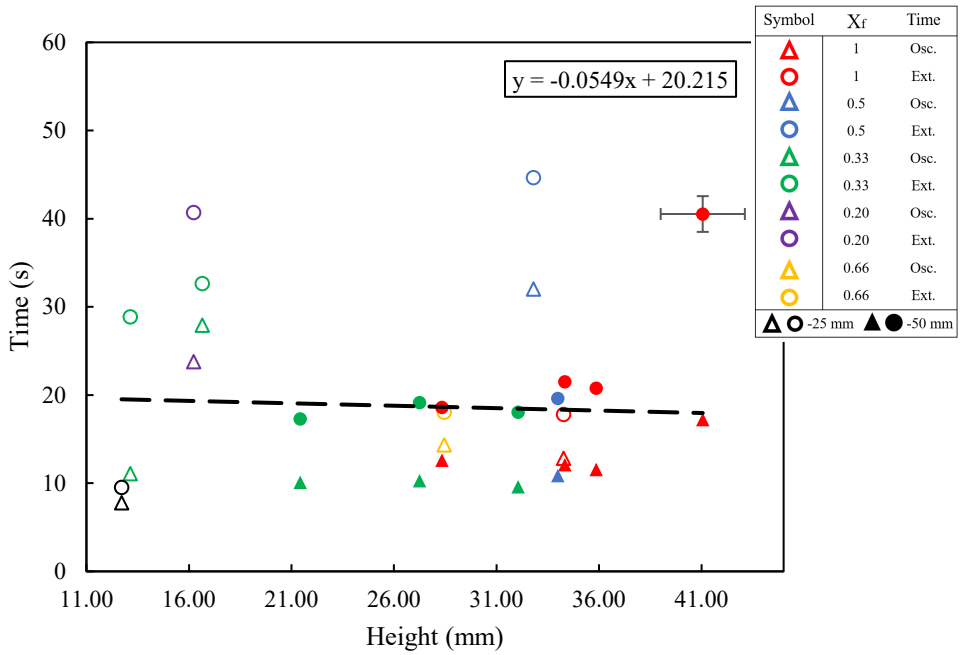

Figure A.16. Extinction and oscillation time relationship with flame height for C_2H_4 with an ambient pressure of 14.7 psia and oxygen mole fraction of 0.25.

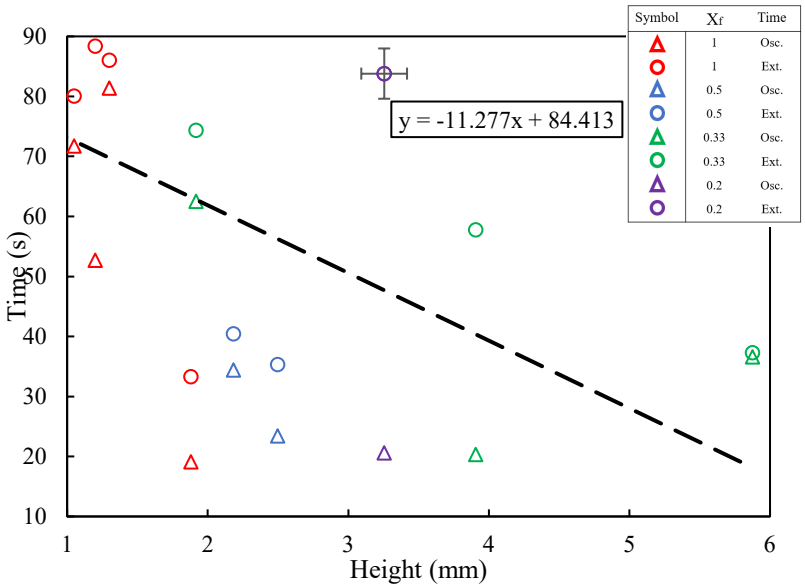

Figure A.17. Extinction and oscillation time relationship with flame height for C_2H_4 with an ambient pressure of 10.2 psia and oxygen mole fraction of 0.27.

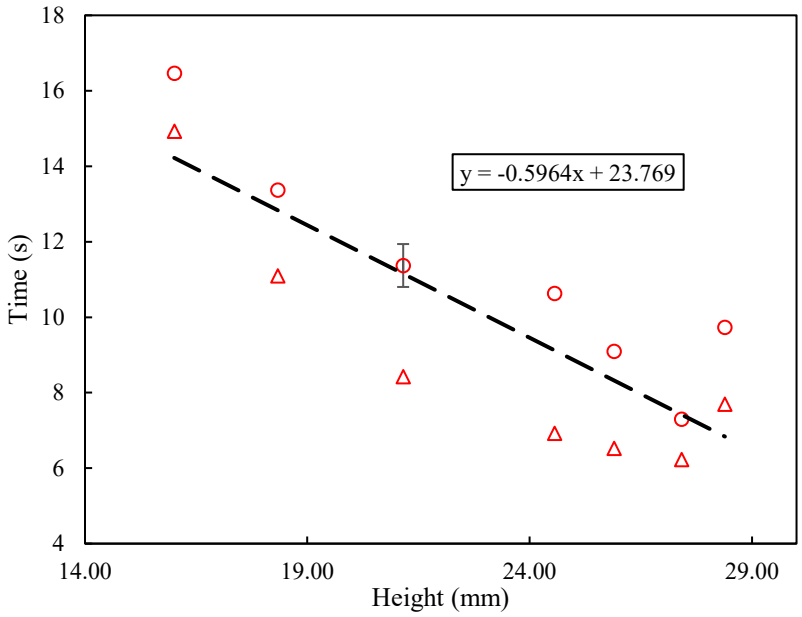

Figure A.18. Extinction and oscillation time relationship with flame height for CH_4 with an ambient pressure of 14.7 psia, oxygen mole fraction of 0.34, and fuel mole fraction of 1.

Appendix B. ISS Data Summary

The summary of ISS parameters including fuel mole fraction, oxygen mole fraction, heat of combustion, pressure, and fuel mass flow rate are shown along with measured heights, oscillation onset, and extinction times in Tables B.1-B.3 below.

Table B.1. ISS Data Summary for C_2H_4 Flames with 25 mm Burner

Test ID	*Xf*	Heat of combustion *kJ/g*	XO2	P *psia*	Mass Flow *mg/s*	Flame Height *mm*	Ext t *s*	Osc t *s*
19063B1	0.50	23.6	0.38	14.7	4.39	62.5	149.33	41
19063C1	0.50	23.6	0.36	14.7	5.96	80	91.5	22.5
19051B1	1.00	47.2	0.33	14.7	1.50	28.8	99.07	58.33
19051C3	1.00	47.2	0.32	14.7	1.88	41.8	65.13	34.3
19051F1	1.00	47.2	0.32	8.2	1.51	37.6	130.23	97.33
19051G1	1.00	47.2	0.30	8.2	1.88	42.9	66.27	44.23
19094H1	1.00	47.2	0.35	8.2	2.67	59.1	46.27	38.73
19094J1	1.00	47.2	0.35	8.2	2.92	58.2	36.9	30.63
19094K1	1.00	47.2	0.35	8.2	3.41	74	36	21.93
19056D3	0.50	23.6	0.33	8.2	3.13	42.6	135.67	60.4
19039C1	1.00	47.2	0.26	14.7	1.88	38.1	25	22.13
19039D1	1.00	47.2	0.25	14.7	1.25	43.5	24.93	22.1
19094F1	1.00	47.2	0.27	10.2	0.81	25.5	132.87	119.5
19094D1	1.00	47.2	0.28	10.2	1.05	30.4	80.07	71.73
19051K1	1.00	47.2	0.25	10.2	1.88	44.6	33.3	19.1
19063F1	0.50	23.6	0.26	14.7	4.37	59.5	32.17	23.03
19063G1	0.50	23.6	0.26	14.7	5.95	72.7	27.67	16.37
19063D1	0.50	23.6	0.27	14.7	2.96	44.1	33.23	19.87
19056B1	0.50	23.6	0.25	14.7	2.19	27.3	37.4	23.9
19056F1	0.50	23.6	0.25	10.2	2.18	28.9	40.43	34.4
19056G1	0.50	23.6	0.24	10.2	2.50	28	35.33	23.4
19094A4	1.00	47.2	0.22	14.7	0.57	18.7	36.97	31.77
19094A2	1.00	47.2	0.22	14.7	0.70	16	30.1	28.27
19094A1	1.00	47.2	0.22	14.7	0.91	21.6	21.4	20
19039H1	1.00	47.2	0.19	14.7	1.50	25	16.07	14.87
19039H2	1.00	47.2	0.18	14.7	1.50	25.5	18	16.37
19039F1	1.00	47.2	0.20	14.7	1.88	33	19.37	18.2
19039G1	1.00	47.2	0.20	14.7	2.52	60	13.23	12.6
19056C1	0.50	23.6	0.22	14.7	2.18	28.1	19.47	14.33
21020B2	0.33	15.7	0.33	8.2	5.88	40.75	61.1	25.83
21020C1	0.33	15.6	0.31	8.2	3.89	32.29	128.43	48.9
20261J1	1.00	47.2	0.29	10.2	1.20	23.92	88.37	52.7
20261J2	1.00	47.2	0.27	10.2	0.96	20.08	76.53	74.5
20261J3	1.00	47.2	0.29	10.2	1.30	23.06	86	81.4
20261H1	0.25	11.9	0.28	10.2	3.26	9.51	83.8	20.6
20261H2	0.26	12.5	0.26	10.2	0.86	25.5	73.63	53.4
21020D1	0.33	15.6	0.28	10.2	1.92	24.61	74.34	62.5
21020F1	0.33	15.7	0.27	10.2	3.91	32.76	57.76	20.3
21020F2	0.33	15.7	0.26	10.2	5.88	42.95	37.27	36.57
20358B1	1.00	47.2	0.39	14.7	1.95	25.56	113.9	63.93
20358D2	1.00	47.2	0.34	14.7	1.95	28.44	66.5	41.3
20358D1	0.50	23.7	0.35	14.7	3.88	32.58	76.13	44.67
20358G6	1.00	47.2	0.24	14.7	1.95	34.27	17.83	12.83
20358G7	0.68	32	0.24	14.7	1.90	28.44	18.07	14.37
20358G1	0.50	23.7	0.25	14.7	1.91	32.79	32.03	13.9
20358G2	0.33	15.5	0.25	14.7	1.91	16.64	32.67	27.94
20358G4	0.33	15.6	0.25	14.7	1.92	13.13	28.87	11.1
20358G3	0.20	9.4	0.25	14.7	1.91	16.22	40.73	23.8
20358G5	0.10	4.6	0.25	14.7	3.90	12.71	9.53	7.8
21020G3	0.33	15.6	0.22	14.7	1.41	19.04	16.44	14.94
21020G4	0.33	15.6	0.22	14.7	1.92	20.22	14.84	13.8
21020G5	0.20	9.3	0.22	14.7	2.91	19.2	12.13	8.4
20346L3	0.33	15.7	0.37	14.7	4.37	23.81	95.13	55.33
20346L3-1	0.33	15.8	0.36	14.7	4.37	24.93	95.23	47.33
20346H1	0.50	23.6	0.25	14.7	1.45	16.15	55.17	45.64
20346H2	0.50	23.6	0.25	14.7	1.45	16.01	55.64	42.67
20346H3	0.33	15.6	0.25	14.7	1.37	11.17	49.37	33.8
20346H4	0.33	15.5	0.25	14.7	1.38	10.25	47	29.13

Table B.2. ISS Data Summary for C2H4 Flames with 50 mm Burner

Test ID	*Xf*	Heat of combustion *kJ/g*	XO2	P *psia*	Mass Flow *mg/s*	Flame Height *mm*	Ext t *s*	Osc t *s*
20247B1	1.00	47.2	0.37	14.7	2.10	30.53	95.47	36.83
20247C1	1.00	47.2	0.35	14.7	2.92	37.35	77.6	24.07
20247D1	1.00	47.2	0.35	14.7	2.95	37.69	74.97	36.8
20247F1	1.00	47.2	0.33	14.7	2.91	35.57	124.13	28.3
20247G1	1.00	47.2	0.30	14.7	2.92	41.88	63.67	25.37
20247L2	1.00	47.2	0.33	14.7	2.91	34.46	136.97	38.6
20247P1	1.00	47.2	0.32	14.7	2.92	42.19	60.5	23.5
20247H2	1.00	47.2	0.25	14.7	2.95	41.06	40.53	17.23
20247J1	1.00	47.2	0.24	14.7	2.92	35.86	20.8	11.57
20247K1	1.00	47.2	0.23	14.7	2.92	34.33	21.53	12.13
20247M1	0.49	23.1	0.31	14.7	4.01	28.4	132.4	33.6
20247N1	0.49	23	0.29	14.7	4.02	28.81	62.77	15.37
21028D1	0.33	15.6	0.35	14.7	5.85	31.2	65.33	25.37
21028D2	0.50	23.6	0.34	14.7	4.88	37.86	49.4	22.43
21028D3	0.66	31.3	0.33	14.7	3.87	33.73	48.4	25.37
21028D4	0.76	36	0.32	14.7	3.38	30.61	49.53	25.5
21028D5	1.00	47.2	0.31	14.7	2.43	35.08	52.67	24.97
21028H1	0.50	23.6	0.25	14.7	5.88	33.98	19.63	10.87
21028G1	0.33	15.6	0.24	14.7	5.85	32.04	18.07	9.63
21028G3	0.33	15.6	0.24	14.7	4.86	27.23	19.17	10.3
21028G5	0.33	15.4	0.24	14.7	3.87	21.42	17.3	10.13
21028G4	1.00	47.2	0.24	14.7	2.43	28.33	18.6	12.63

Table B.3. ISS Data Summary for CH4 Flames with 25 mm Burner

Test ID	*Xf*	Heat of combustion *kJ/g*	XO2	P *psia*	Mass Flow *mg/s*	Flame Height *mm*	Ext t *s*	Osc t *s*
20279B1	1.00	50.1	0.39	14.7	0.97	14.81	25.6	22.47
20279B2	1.00	50.1	0.38	14.7	0.86	14.39	30.6	27.23
20279B4	1.00	50.1	0.38	14.7	1.21	19.17	24.1	17.17
20279B5	1.00	50.1	0.37	14.7	2.44	25.53	42.3	7.8
20279B6	1.00	50.1	0.37	14.7	1.95	22.83	18.43	7.83
20279B7	1.00	50.1	0.36	14.7	2.93	30.4	14.93	7.7
20279B8	1.00	50.1	0.35	14.7	2.20	29.76	42.7	9.43
20339L1	0.71	29	0.37	14.7	1.70	19.8	17.27	14.5
20339L2	0.70	28.8	0.37	14.7	2.57	21.35	13.23	8.73
20339L3	0.70	28.8	0.37	14.7	3.89	26.47	8.13	6.76
20339A2	0.50	18.3	0.39	14.7	2.91	17.63	19.2	16.33
20339A3	0.50	18.1	0.39	14.7	5.84	28.16	10.87	7.2
20339A4	0.50	18.2	0.39	14.7	4.38	22.33	15	7.5
20339A6	0.50	18.2	0.38	14.7	3.66	21.35	23.1	9.23
20339A8	0.50	18.4	0.38	14.7	3.15	18.26	24.27	10.87
20339A9	0.50	18.3	0.37	14.7	3.13	20.37	25.3	18.53
20339A0	0.71	29.2	0.38	14.7	1.71	15.92	16.87	14.9
20279D1	1.00	50.1	0.35	14.7	1.46	21.15	11.37	8.43
20279D2	1.00	50.1	0.34	14.7	1.95	24.56	10.63	6.93
20279D3	1.00	50.1	0.34	14.7	2.45	28.39	9.73	7.7
20279D4	1.00	50.1	0.34	14.7	2.93	27.41	7.3	6.23
20279D5	1.00	50.1	0.33	14.7	0.97	16.01	16.47	14.93
20279D6	1.00	50.1	0.33	14.7	1.21	18.33	13.37	11.1
20279D7	1.00	50.1	0.33	14.7	2.21	25.9	9.1	6.53
20279J1	1.00	50.1	0.25	14.7	0.97	17.36	6.67	6.1
20279J2	1.00	50.1	0.25	14.7	0.86	14.92	5.87	5.87
20279J6	1.00	50.1	0.24	14.7	1.95	17.4	21.43	6.97
20339J3	0.50	18.2	0.25	14.7	2.87	20.93	5.5	5.44

Appendix C. Converting ACME HOBJ Files to Color Images

The detailed process of converting the HOBJ images into viewable JPEGS and TIFFS using OMA2, as well as the process of making the images into image sequence videos, is described below.

The ACME camera on the ISS took images of the flame tests based on a specified exposure and gain. It generated the images in the HOBJ format. To analyze the flame behavior, the HOBJ files needed to be converted to readable color images – either JPEGS or TIFFS. OMA2 software was used for this conversion. A macro was created on OMA2 to easily convert series of images at once.

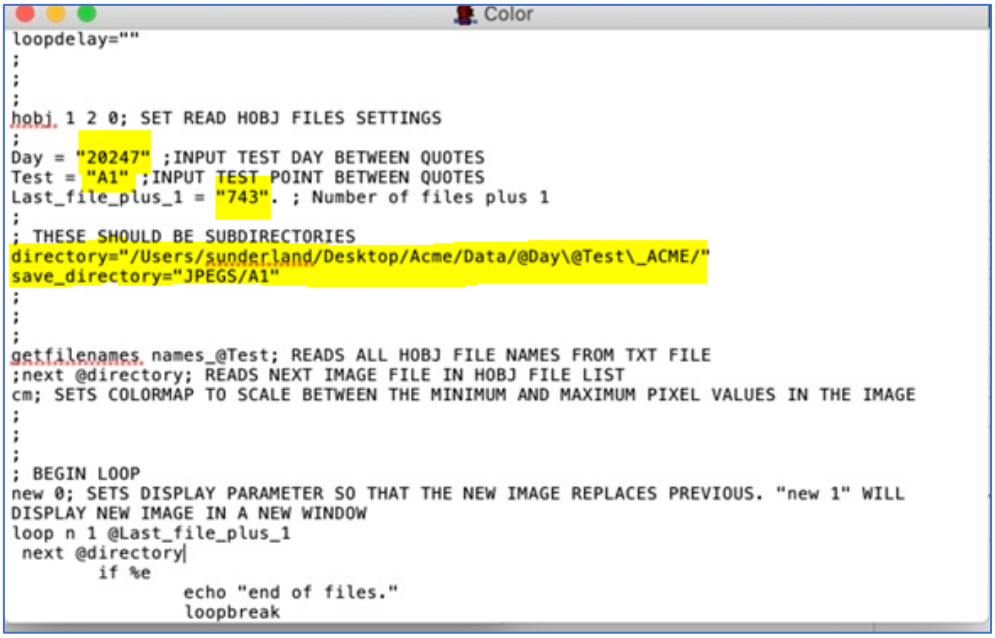

Figure C.1. Sample image of OMA2 macro used to convert HOBJ files from ACME camera into color images.

Converted TIFF images could then be used to analyze flame temperatures and converted JPEG images could be used to create image sequences used to illustrate the flame's oscillation

and extinction behavior. Adobe Premiere Pro was used to combine the images into an image sequence.

References

[1] B. Burrough, Dragonfly: NASA and the Crisis Aboard the MIR. Harper Collins. 1998.

[2] NASA-STD-6001B. Flammability, off gassing, and compatibility requirements and test procedures, 2016.

[3] A. Markan, "Development and analysis of a burning rate emulator (BRE) for study in microgravity," 2018.

[4] NASA, "ACME-SRD-001.B Integrated Science Requirements Document (ISRD)," Advanced combustion via microgravity experiments, 2013.

[5] F. V. Lundstrom, P. B. Sunderland, J. G. Quintiere, P. van Hees and J. L. de Ris, "Study of ignition and extinction of small-scale fires in experiments with an emulating gas burner," Fire Safety Journal, vol. 87, pp. 18-24, 2017.

[6] F. V. Plathner, J. G. Quintiere and P. van Hees, "Analysis of extinction and sustained ignition," Fire Safety Journal, vol. 105, pp. 51-61, 2019

[7] M. J. Bustamante, "Experimental investigation of liquid and gas fueled flames toward the development of a burning rate emulator (BRE) for microgravity applications," 2012.

[8] Y. Zhang, M. Kim, H. Guo, P. B. Sunderland, J. G. Quintiere, J. de Ris and D. P. Stocker, "Emulation of condensed fuel flames with gases in microgravity," Combustion and Flame, vol. 162, pp. 3449-3455, 2015

[9] M. Kim, "Procedures to obtain accurate measurement from a gas fueled burner," 2014.

[10] A. Markan, P. B. Sunderland, J. G. Quintiere, J. L. de Ris, D. P. Stocker and H. R. Baum, "A burning rate emulator (BRE) for study of condensed fuel burning in microgravity," Combustion and Flame, vol. 192, pp. 272-282, 2018

[11] R. C. Corlett, "Heat Transfer Data Summary -Pool Burning Study," National Science Foundation, 1965

[12] R. C. Corlett, "Gas fires with pool-like boundary conditions," Combustion and Flame, vol. 12, no. 1, pp. 19-32, 1968.

[13] R. C. Corlett, "Gas fires with pool-like boundary conditions: further results and interpretation," Combustion and Flame, vol. 14, pp. 351-360, 1970

[14] J. de Ris and L. Orloff, "A Dimensionless Correlation of Pool Burning Data," Combustion and Flame, vol. 18, pp. 381-388, 1972.

[15] J. L. de Ris and L. Orloff, "The role of buoyancy direction and radiation in turbulent diffusion flames on surfaces," Symposium (International) on Combustion, vol. 15, no. 1, pp. 175-182, 1975.

[16] J.S. Kim, J.L. De Ris, and F.W. Kroesser. Laminar free-convective burning of fuel surfaces. 13(1):949–961, 1971.

[17] T. Wilcutt and W. B. Harkins, “Trial by Fire: Space Station Mir: On-Board Fire,” in *Nasa.gov*, 2021.

[18] ISO 5660-1. Reaction-to-fire tests-heat release, smoke production and mass loss rate-part 1: heat release rate (cone calorimeter method), 2002.

[19] G.A. Ruff, D.L. Urban, M.D. Pedley, and P.T. Johnson. Safety design for space systems. Fire Safety, 2009.

[20] J.S. T’ien. The possibility of a reversal of material flammability ranking from normal gravity to microgravity. Combustion and Flame, 80(3):355–357, 1990.

[21] Lecoustre, V., Narayanan, P., Baum, H. R. and Trouvé, A. (2011) “Local extinction of diffusion flames in fires”, Fire Safety Science – Proc. Tenth International Symposium, International Association for Fire Safety Science, 583-595.

[22] Law, C.K., Combustion Physics, Cambridge University Press, 2006.

[23] D.L. Urban, D.P. Stocker, R.L. Axelbaum, *Radiative Extinction of Gaseous Spherical Diffusion Flames in Microgravity,* Combustion and Flame 151 (2007) 665-675.

[24] P. Dehghani, P. B. Sunderland, J. G. Quintiere, and J. L. de Ris, “Burning in microgravity: Experimental results and analysis,” *Combustion and Flame*, vol. 228, pp. 315–330, 2021.

[25] E. Auth, “Using a Burning Rate Emulator (BRE) to Emulate Condensed Fuels and Study Pool Fire Behavior in 1G,” Thesis, Digital Repository at the University of Maryland, 2019.